

## New tailored substituted–benzothiazole Schiff base Cu(II)/Zn(II) antitumor drug entities: Effect of substituents on DNA binding profile, antimicrobial and cytotoxic activity

Sifteen Zehra, Mohammad Shavez Khan, Iqbal Ahmad & Farukh Arjmand

To cite this article: Sifteen Zehra, Mohammad Shavez Khan, Iqbal Ahmad & Farukh Arjmand (2018): New tailored substituted–benzothiazole Schiff base Cu(II)/Zn(II) antitumor drug entities: Effect of substituents on DNA binding profile, antimicrobial and cytotoxic activity, Journal of Biomolecular Structure and Dynamics, DOI: [10.1080/07391102.2018.1467794](https://doi.org/10.1080/07391102.2018.1467794)

To link to this article: <https://doi.org/10.1080/07391102.2018.1467794>



Accepted author version posted online: 20 Apr 2018.



Submit your article to this journal [↗](#)



View related articles [↗](#)



View Crossmark data [↗](#)

**Publisher:** Taylor & Francis

**Journal:** *Journal of Biomolecular Structure and Dynamics*

**DOI:** <http://doi.org/10.1080/07391102.2018.1467794>



**New tailored substituted–benzothiazole Schiff base Cu(II)/Zn(II) antitumor drug entities: Effect of substituents on DNA binding profile, antimicrobial and cytotoxic activity**

Sifteen Zehra<sup>a</sup>, Mohammad Shavez Khan<sup>b</sup>, Iqbal Ahmad<sup>b</sup> and Farukh Arjmand<sup>a,\*</sup>

<sup>a</sup> Department of Chemistry, Aligarh Muslim University, Aligarh 202002, Uttar Pradesh, India

<sup>b</sup> Department of Agricultural Microbiology, Aligarh Muslim University, Aligarh 202002, Uttar Pradesh, India

\*Corresponding author. E-mail address: farukh\_arjmand@yahoo.co.in (F. Arjmand).

\*Corresponding author. Tel.: +91 5712703893.

**Abstract**

New tailored Cu(II) & Zn(II) metal–based antitumor drug entities were synthesized from substituted benzothiazole *o*–vanillin Schiff base ligands. The complexes were thoroughly characterized by elemental analysis, spectroscopic studies {IR, <sup>1</sup>H & <sup>13</sup>C NMR, ESI–MS, EPR} and magnetic susceptibility measurements. The structure activity relationship (SAR) studies of benzothiazole Cu(II) & Zn(II) complexes having molecular formulas [C<sub>30</sub>H<sub>22</sub>CuN<sub>5</sub>O<sub>7</sub>S<sub>2</sub>],

[C<sub>30</sub>H<sub>20</sub>Cl<sub>2</sub>CuN<sub>5</sub>O<sub>7</sub>S<sub>2</sub>], [C<sub>30</sub>H<sub>20</sub>CuF<sub>2</sub>N<sub>5</sub>O<sub>7</sub>S<sub>2</sub>], [C<sub>30</sub>H<sub>22</sub>N<sub>4</sub>O<sub>4</sub>S<sub>2</sub>Zn], [C<sub>30</sub>H<sub>20</sub>Cl<sub>2</sub>N<sub>4</sub>O<sub>4</sub>S<sub>2</sub>Zn] and [C<sub>30</sub>H<sub>20</sub>F<sub>2</sub>N<sub>5</sub>O<sub>7</sub>S<sub>2</sub>Zn], with CT-DNA were performed by employing absorption, emission titrations and hydrodynamic measurements. The DNA binding affinity was quantified by  $K_b$  and  $K_{sv}$  values which gave higher binding propensity for chloro substituted Cu(II) [C<sub>30</sub>H<sub>20</sub>Cl<sub>2</sub>CuN<sub>5</sub>O<sub>7</sub>S<sub>2</sub>] complex, suggestive of groove binding mode with subtle partial intercalation. Molecular properties and drug likeness profile were assessed for the ligands and all the Lipinski's rules were found to be obeyed. The antimicrobial potential of ligands and their Cu(II) & Zn(II) complexes were screened against some notably important pathogens *viz.*, *E. coli*, *S. aureus*, *P. aeruginosa*, *B. subtilis* and *C. albicans*. The cytotoxicity of the complexes [C<sub>30</sub>H<sub>20</sub>Cl<sub>2</sub>CuN<sub>5</sub>O<sub>7</sub>S<sub>2</sub>], [C<sub>30</sub>H<sub>20</sub>CuF<sub>2</sub>N<sub>5</sub>O<sub>7</sub>S<sub>2</sub>], [C<sub>30</sub>H<sub>20</sub>Cl<sub>2</sub>N<sub>4</sub>O<sub>4</sub>S<sub>2</sub>Zn] and [C<sub>30</sub>H<sub>20</sub>F<sub>2</sub>N<sub>5</sub>O<sub>7</sub>S<sub>2</sub>Zn] were evaluated against five human cancer cell lines *viz.*, MCF-7 (breast), MIA-PA-CA-2 (pancreatic), HeLa (cervix) and Hep-G2 (Hepatoma) and A498 (Kidney) by SRB assay which revealed that chloro substituted [C<sub>30</sub>H<sub>20</sub>Cl<sub>2</sub>CuN<sub>5</sub>O<sub>7</sub>S<sub>2</sub>] complex, exhibited pronounced specific cytotoxicity with GI<sub>50</sub> value of 4.8 µg/ml against HeLa cell line. Molecular docking studies were also performed to explore the binding modes and orientation of the complexes in the DNA helix.

**Keywords:** Benzothiazole Cu(II) & Zn(II) Schiff base complexes; structure activity relationship; antimicrobial studies; cytotoxicity; molecular docking.

## 1. Introduction

*N*-heterocycles *viz.*, benzimidazole, benzothiazole, indole, pyrazole and quinolines etc. have emerged as an important distinct class of anticancer therapeutic agents (D. Kumar & Kumar, 2016). These compounds possess *N*-heterocyclic aromatic pharmacophore synthon which is responsible for harnessing medicinal properties by multiple mechanisms which may be largely responsible for inhibiting cell growth and inducing apoptosis (Solomon, Hu & Lee, 2009). FDA's Center for Drug Evaluation and Research (CDER) approves a wide range of new molecular entities (NMEs) possessing bioactive moieties which may provide important new therapies for treating patients with many chronic diseases. Many prominent *N*-heterocyclic compounds developed by reputed pharmaceutical companies (Pfizer, AstraZeneca, Novartis etc.) have been approved by US FDA as anticancer agents for myriad phenotypes of cancers (<http://www.fda.gov>). Unfortunately, many of these NMEs fail either in clinical trials or in the developmental stages due to issues of systemic toxicity and low absorption at cellular levels. Among the *N*-heterocycles, benzothiazole derivatives have gained prominence due to diverse biological activities *viz.*, antimicrobial, antiviral and anticancer activities (Racan  et al., 2013). Besides this, benzothiazole is a key component of nucleic acids and therefore, can participate directly in encoding of genetic information. Being an important drug synthon, it can be tethered to other organic ancillary ligands for targeted therapy to yield more efficacious and potent ligand scaffolds. Several benzothiazole derivatives are reported to possess excellent *in vitro* and *in vivo* cytotoxicity at low nanomolar concentrations (Prota et al., 2014). Literature reports reveal that 2-aminobenzothiazole derivatives were synthesized and tested at National Cancer Institute (NCI) against nine panels of cancer cell lines for antitumor activity. It was observed that chloro derivative, 7-chloro-*N*-(2,6-dichlorophenyl)benzo[d]thiazol-2-amine was most active against non-small lung cancer cell line, HOP-92 with significantly good GI<sub>50</sub> value of

$7.18 \times 10^{-8}$  M (Noolvi Patel & Kaur, 2012). Furthermore, modifications of the benzothiazole scaffold could yield improved cytotoxicity profile which has been demonstrated in a series of 2-anilinopyridinyl-benzothiazole Schiff base conjugates reported by A. Kamal *et al.* The inhibitory effects of varied magnitude against the tested cell lines ( $>20 \mu\text{M}$ – $100 \mu\text{M}$  concentration) were observed. Interestingly, these conjugates have displayed specificity toward the prostate cancer cell line (DU145) and most of them have demonstrated significant cytotoxic activity (Shaik et al., 2017).

Most of the chemotherapeutics in clinical use for the treatment of cancer show toxicity due to off-target uptake in the cells in biological system. Many researchers in the area of inorganic medicinal chemistry are making considerable efforts to achieve the goal of antitumor drugs with reduced toxicities. Among the rational therapeutic approaches to develop new metal-based biologically active compounds, strategies using transition metal complexes {Co(II), Cu(II) & Zn(II)} are in frontline exhibiting improved pharmacological profile (Renfrew, 2014).

Furthermore, the synergy between the metal ions and ligand scaffold would result in a more bioactive therapeutic agent capable of selective targeted activity at the site of action, leaving normal or healthy cells unaffected. In this research work, we have opted for a rational synthetic approach in which a benzothiazole active pharmacophore synthon was used to obtain Schiff base complexes which could be predicted for antimicrobial chemotherapy which is newly conceived concept as it can furnish therapeutic entities showing both superior antimicrobial potency as well as pronounced anticancer activity.

Schiff-bases are privileged ligand scaffolds exhibiting a wide range of applications in the field of medicinal inorganic chemistry (Hameed, Rashida, Uroos, Ali & Khan, 2017). They have been categorized as versatile ligand moieties due to their structural stability, synthetic flexibility

and excellent chelating ability with metal ions (Shahraki & Heydari, 2017). They are endowed with potential biological and pharmacological activities such as antimicrobial (Jana, Dalapati & Guchhait, 2012; Biswas et al., 2012), anti-malarial (Facchinetti, Reis, Gomes & Vasconcelos 2012), antioxidant (Dehkhodaeia, Sahihia & Rudbari, 2017) and anticancer (Amiri et al., 2017). In addition, Schiff bases are utilized as chemical and stereo selective DNA structural probes, mimicking the active sites in the biological system and DNA dependent electron transfer processes (Shokohi-pour, Chiniforoshan, Sabzalian, Esmaeili, Abbas & Borojeni). Schiff base transition complexes modulated with several heterocyclic moieties such as pyrazole, 1,2,4-triazoles, coumarins, benzothiazole and benzoxazoles are of remarkable interest due to exclusive properties associated with the heterocyclic pharmacophore synthon, which finds application in the treatment of chronic diseases *viz.*, HIV-AIDS, tuberculosis, Alzheimer's and cancer with multiple etiologies (Jadhao et al., 2017; Creaven et al., 2010; Kumar et al., 2017). Heterocyclic Schiff base transition metal complexes are of prominent importance due to their efficient and enhanced bioactivity against a wide range of bacterial and fungal strains (Manjunath, Kulkarni, Bagihalli, Malladi & Patil, 2017; Hranjec et al., 2011). A series of novel bioactive Schiff base transition metal complexes derived from 8-formyl-7hydroxy-4-methylcoumarin and 2-hydrazino benzothiazole have been synthesized and thoroughly characterized. The metal complexes are screened for their bacterial and fungal activity and were found to be more active than the free ligand. The cytotoxic activity of the metal complexes was evaluated against human ovarian cancer cell line (PA-1) and they are found to be non-toxic against the tested cell line. Preliminary screening of the metal complexes against the antitubercular activity displayed a significantly low MIC value of 0.8µg/ml as compared to the standard drug and free ligand (Jawoor, Patil & Toragalmath, 2018).

Incorporating metal ions in bioactive ligand scaffolds can furnish 'metallo-drug' chemotherapeutics which are supposed to exert their effect by inhibition of proteins and enzymes, and catalyze various intracellular processes, enhance lipophilicity and cell permeation, alteration of cell membrane functions and arrest of cell cycle etc. (Tan, Lu, Ji & Mao, 2014). Among the transition metals, copper complexes have emerged as a notably important class of cancer therapeutics (Santini et al., 2014). In contrast to Pt drugs that are covalently bound to DNA nucleobases, Cu(II) complexes primarily form noncovalent interactions with DNA either by electrostatic surface binding to the oxygen atoms of negatively charged DNA phosphodiester helix or groove binding (both major or minor) and intercalation (Gama et al., 2014). Advances in chemistry of copper anticancer therapeutic agents have shown that many copper complexes with diverse ligand topology Schiff base, peptides, amino acids, terpyridines, polypyridyls etc. demonstrate excellent cytotoxicity against a wide spectrum of cancer phenotypes including the cisplatin resistant strains (Tardito et al., 2011; Manikandamathavan et al., 2014; Yu et al., 2011; Nagababu et al., 2015; Goswami, Chakravarthi, Roy, Karande & Chakravarty, 2011; Maity et al., 2010). Two copper complexes have entered the clinical trials (Galindo–Murillo, García–Ramos, Ruiz–Azuara, III Cheatham & Cortés–Guzmán, 2015) and as copper complexes exhibit a different mechanism of action as compared to classical Pt drugs, it is expected that the major challenge of chemoresistance can be successfully overcome. Being a bioessential less toxic element, copper (II) complexes are believed to overcome membrane transportation, multi–resistance and toxicity issues (McGivern, Afsharpour & Marmion, 2017). A newly envisaged design of antimicrobial copper–based therapeutic agent was reported by Hassan *et al.* They prepared a water–soluble, copper–containing terpyridine carboxymethyl cellulose complex which demonstrated good antimicrobial activity and showed inhibition of the

growth of the Gram-positive bacteria and the fungus as well as 90% of the Gram-negative bacteria at 8 mg/mL. Such new antimicrobial metallo-therapeutics are being developed to prevent and treat these drug-resistant infections (E. A. Hassan, Hassan, Moorefield & Newkome, 2015). Another important potential transition metal of interest is Zn(II) which is endowed by distinctive properties to undergo Lewis activation, generation of nucleophiles and regulating apoptosis. Zinc plays an important role in the regulation of various cellular processes *viz.*, DNA synthesis, gene expression, enzyme synthesis and catalytic functions (Mendiguchia, Pucci, Mastropietro, Ghedini & Crispini, 2013). Besides this Zn(II) complexes exhibit low *in vivo* cytotoxicity and new multimodes of action and cellular targets (Tan Wang & Zhu, 2009). The novelty of Zn(II) complexes as potent anticancer therapeutics could be due to structural stability that may be induced by changing the coordination sphere *in vivo*.

In our laboratory, strenuous efforts are being made to achieve efficacious metal-based chemotherapeutic drug candidates for treating cancer. In continuation to our pursuit for the design of smart metal-based drug entities, we have prepared a novel series of substituted benzothiazole-*o*-vanillin Schiff base Cu(II) & Zn(II) complexes. Substituents of different nature such as chloro, fluoro along with unsubstituted one were used to study their effect on anticancer and antimicrobial activity. The structure activity relationship (SAR) is helpful to access NMEs and such functionalization of the bioactive benzothiazole scaffolds can throw light on mechanistic insight for specific targeted therapies. Due to multi-drug resistance, there is a substantial need for the development of newer potential antimicrobial chemotherapeutic drug entities endowed with improved mechanism of action and multifold enhanced activity.

## **2. Experimental Section**

### **2.1. Materials and methods**

*o*-vanillin, 2-Aminobenzothiazole, 2-Amino-4-chlorobenzothiazole, and 2-Amino-6-fluorobenzothiazole (Sigma Aldrich),  $\text{Cu}(\text{NO}_3)_2 \cdot 2\text{H}_2\text{O}$  and  $\text{Zn}(\text{CH}_2\text{COO})_2 \cdot 2\text{H}_2\text{O}$  (Merck) were used as received. Calf thymus DNA (CT-DNA) and Tris(hydroxymethyl)aminomethane or Tris Buffer, were purchased from Sigma Chemicals Co. All reagents and solvents were of best commercial grade and were used without further purification.

Elemental analyses were performed on Carlo Erba Analyser Model 1106. Molar conductance was measured at room temperature on a Digisun Electronic conductivity Bridge. Fourier transforms IR (FTIR) spectra were recorded on an Interspec 2020 FTIR spectrometer. Electronic spectra were recorded on UV-1700 PharmaSpec UV-vis spectrophotometer (Shimadzu). Fluorescence measurements were made on Shimadzu RF-5201 fluorescence spectrophotometer. The EPR spectra of the copper complex was obtained on Varian E 112 EPR spectrometer using X band frequency (9.1 GHz) at room temperature in solid state. Magnetic moment measurements were carried out using Sherwood scientific magnetic susceptibility balance at 25°C. The  $^1\text{H}$  and  $^{13}\text{C}$  NMR spectra were obtained on a Bruker Avance DRX-400 spectrometer operating at room temperature. Electrospray mass spectra were recorded on Micromass Quattro II triple quadrupole mass spectrometer. The viscosity measurements were carried out by using Ostwald capillary viscometer at 25°C.

## **2.2. Synthesis**

### *2.2.1. Synthesis of ligands*

The ligand L1-L3 were synthesized by adding *o*-vanillin (0.152 g, 1 mmol) to a stirred methanolic solution (10 ml) of 2-aminobenzothiazole (0.150 g, 1 mmol), 2-amino-4-chlorobenzothiazole (0.184 g, 1 mmol) and 2-amino-6-fluorobenzothiazole

(0.168 g, 1 mmol), respectively in a 1:1 M ratio (Fig.1). The reaction mixtures were refluxed for 2 h and the progress of reaction was monitored by TLC. The yellow precipitate which formed was filtered off under vacuum, washed thoroughly with methanol and dried *in vacuo*.

### 2.3.2. Synthesis of complexes **1** and **2** (a–c).

The complexes **1** and **2** (a–c) were synthesized by adding methanolic solution of  $\text{Cu}(\text{NO}_3)_2 \cdot 2\text{H}_2\text{O}$  (0.241 g, 1 mmol) and  $\text{Zn}(\text{CH}_2\text{COO})_2 \cdot 2\text{H}_2\text{O}$  (0.241 g, 1 mmol) to a methanolic solution of ligands **L1** (0.284 g), **L2** (0.318 g), **L3** (0.303 g), (1 mmol) in a 1:2 molar ratio which was stirred for 2 h at room temperature to obtain brown and orange colored precipitates, respectively.

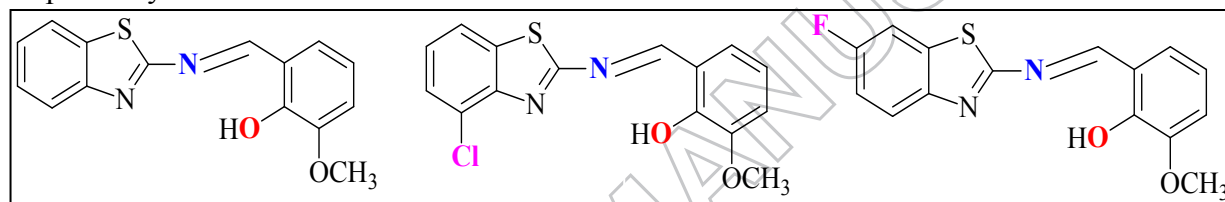


**Fig.1.** Structure of the substituted benzothiazole derived ligands **L1–L3**.

### 2.3. DNA binding studies

DNA binding studies, including absorption, fluorescence, emission titrations and viscosity measurements conformed to the standard methods previously reported by our laboratory (Lakowicz & Webber, 1973; Wolfe, Shimer & Meehan, 1987; Arjmand, Muddassir, Zaidi & Ray, 2013) were carried out.

Absorption titration were performed by maintaining the constant complex concentration ( $1.67 \times 10^{-4}$  M) and varying the concentration of the CT–DNA ( $0.00–5.0 \times 10^{-5}$  M). Fluorescence quenching experiments were carried out by concomitant addition of metal complexes to the EB–DNA and DAPI–DNA system such that  $[\text{complex}]/[\text{DNA}] = 1 : 1$  to  $8 : 1$  in 5 mM Tris–HCl/50 mM NaCl buffer (pH = 7.2). While measuring the spectra, an equal amount of DNA

was added to both the complex and the reference solution to eliminate the absorbance of the CT–DNA, and Tris–HCl buffer was subtracted through base line correction.

Viscosity measurements were carried out using Ostwald viscometer. The viscosity of CT–DNA in buffer solution was measured in the presence of increasing amounts of the complexes (up to the value of  $r = 1.0$ ) at room temperature. The flow time was measured using a digital stopwatch. Data are presented as  $(\eta/\eta_0)^{1/3}$  vs. the ratio of the concentration of complex to DNA, where  $\eta$  is the viscosity of CT–DNA in the presence of compound and  $\eta_0$  is the viscosity of CT–DNA alone. Viscosity values were calculated according to the relation  $\eta = (t - t_0)/t_0$ , where  $t$  was the flow time of the CT–DNA solution in the presence or absence of the complex and  $t_0$  of the buffer alone. The average values were replicated thrice to evaluate the viscosity of the complexes.

## 2.5. Antimicrobial studies

All the synthesized ligands L1–L3 and their complexes **1** and **2** (a–c) were screened for their *in vitro* antibacterial activity against two Gram–negative [*Escherichia coli* (ATCC 25922), *Pseudomonas aeruginosa* (ATCC 27853)] and two Gram–positive [*Staphylococcus aureus* (ATCC 25923) and *Bacillus subtilis* (MTCC 121)] bacterial strains. The agar well diffusion method of Perez *et al.*, also described earlier by Ahmad *et al.* was adopted for measuring the antibacterial assays. Briefly, all cultures were routinely maintained on NA (nutrient agar) and incubated at 27 °C for overnight in NB (Nutrient broth). After incubation, 0.1 ml aliquot of bacterial culture was spread uniformly with the help of spreader on NA plates. Wells of 8 mm diameter were punched into the agar medium, sealed with soft agar and loaded with different concentrations of the metal complexes (0.1 ml). Antibiotic disc, Doxycycline (30 mcg/disc) and solvent were used as positive and negative control, respectively. The plates were then incubated

for 24 h at 37 °C and the resulting zones of inhibition (mm) were measured. The inoculums of non-spore forming fungi, *Candida albicans* was obtained by growing in SD (Sabouraud Dextrose) broth at 28 °C for 48 h. Volume of 0.1 ml of diluted fungal cell suspension was uniformly spread on SDA (Sabouraud Dextrose Agar) plates and test compound were loaded into wells (describe above). *C. albicans* plates were incubated at 27 °C for 18–48 h and antifungal activity was determined by measuring the diameters of the inhibition zone (mm).

### **2.6. *In vitro* cytotoxic assay**

The *in vitro* anticancer activity of **1** and **2** (b & c) was carried out against five human cancer cell lines of different histological origin *viz*; MCF-7 (breast), MIA-PA-CA-2 (pancreatic), HeLa (cervix), Hep-G2 (Hepatoma) and A498 (Kidney). G-Adriamycin, a standard anticancer drug, was taken as the control. The cell lines were procured and grown in RPMI-1640 medium supplemented with 10% Fetal Bovine Serum (FBS) and antibiotics to study growth pattern of these cells. The proliferation of the cells upon treatment with chemotherapy was determined by means of the Sulphorhodamine-B (SRB) assay. All cell lines were seeded into 96 well plates and cells were counted and cell counts was adjusted according to the titration readings so as to give optical density in the linear range (0.5 to 1.8) and were incubated at 27 °C in CO<sub>2</sub> incubator for 24 h. The stock solution of the complexes were prepared as 100 mg/ ml in DMSO and four dilutions i.e. 10 µg/ml, 20 µg/ml, 40 µg/ml, 80 µg/ ml, in triplicates were tested, each well receiving 90 µl of cell suspension. The plates were labeled and were incubated for 48 h. Termination of experiment was done by gently layering the cells with 50 µl of chilled 20% TCA (in case of adherent cells) and 50% TCA (in case of suspension cell lines) for cell fixation and kept at 4°C for 1 h. Plates stained with 50 µl of 0.4% SRB for 20 min. All experiments were made in triplicate.

## 2.7. Structure–activity relationship studies

In order to demonstrate the structure–activity relationship (SAR) and quantitatively estimate the molecular properties of the ligands and their respective metal complexes, the molinspiration calculations were carried out ([www.molinspiration.com](http://www.molinspiration.com)).

## 2.8. Molecular docking studies

Molecular docking studies were performed by using HEX 8.0 software (Macindoe, Mavridis, Venkatraman, Devignes & Ritchie, 2010), a molecular graphics program for calculating and displaying feasible docking modes of DNA molecule. Structure of the complexes was sketched by Chemdraw, energy minimized and converted into PDB format using Mercury software (<http://www.ccdc.cam.ac.uk/>). The crystal structure of the B–DNA dodecamer d(CGCGAATTCGCG)<sub>2</sub> (PDB ID: 1BNA) were downloaded from the protein data bank (<http://www.rcsb.org./pdb>). Visualization of the docked pose was done by using Discovery Studio molecular graphics program.

## 3. Results and discussions

All the ligands L1–L3 and their respective metal complexes **1** and **2** (a–c) are found stable at room temperature and are soluble in common organic solvents *viz.*, methanol, ethanol, DMF and DMSO. The molar conductance values (9.5–12.8  $\Omega^{-1} \text{ cm}^2 \text{ mol}^{-1}$ ) are too low to account for any dissociation of the complexes, indicating that the complexes are non–electrolytes (Geary, 1971). On the basis of spectral and magnetic studies, the coordination geometry of copper(II) [ $\text{C}_{30}\text{H}_{22}\text{CuN}_5\text{O}_7\text{S}_2$ ], [ $\text{C}_{30}\text{H}_{20}\text{Cl}_2\text{CuN}_5\text{O}_7\text{S}_2$ ] and [ $\text{C}_{30}\text{H}_{20}\text{CuF}_2\text{N}_5\text{O}_7\text{S}_2$ ] and zinc(II) [ $\text{C}_{30}\text{H}_{22}\text{N}_4\text{O}_4\text{S}_2\text{Zn}$ ], [ $\text{C}_{30}\text{H}_{20}\text{Cl}_2\text{N}_4\text{O}_4\text{S}_2\text{Zn}$ ] and [ $\text{C}_{30}\text{H}_{20}\text{F}_2\text{N}_5\text{O}_7\text{S}_2\text{Zn}$ ] complexes were proposed to be square pyramidal and tetrahedral, respectively (Fig. S1).

IR spectra of ligands L1–L3 showed a characteristic band at 3434–3435  $\text{cm}^{-1}$  assigned to phenolic (OH) group which was found absent in the spectra of complexes [ $\text{C}_{30}\text{H}_{22}\text{CuN}_5\text{O}_7\text{S}_2$ ],

[C<sub>30</sub>H<sub>20</sub>Cl<sub>2</sub>CuN<sub>5</sub>O<sub>7</sub>S<sub>2</sub>] [C<sub>30</sub>H<sub>20</sub>CuF<sub>2</sub>N<sub>5</sub>O<sub>7</sub>S<sub>2</sub>] [C<sub>30</sub>H<sub>22</sub>N<sub>4</sub>O<sub>4</sub>S<sub>2</sub>Zn], [C<sub>30</sub>H<sub>20</sub>Cl<sub>2</sub>N<sub>4</sub>O<sub>4</sub>S<sub>2</sub>Zn] and [C<sub>30</sub>H<sub>20</sub>F<sub>2</sub>N<sub>5</sub>O<sub>7</sub>S<sub>2</sub>Zn], indicating its coordination to metal ion *via* deprotonation (Daravath et al., 2017). A significant shift was observed in the absorption frequency of azomethine group  $\nu(\text{C}=\text{N})$  in ligands at 1632–1635 cm<sup>-1</sup> as compared to the metal complexes 1645–1640 cm<sup>-1</sup>, thereby validating its coordination *via* the nitrogen atom (Bhowmik et al., 2016). In addition, medium intensity bands were also observed for complexes **1** and **2** (a–c) in the region 542–468 and 438–420 cm<sup>-1</sup> attributed to the stretching frequency of  $\nu(\text{Cu}/\text{Zn}-\text{O})$  and  $\nu(\text{Cu}/\text{Zn}-\text{N})$  vibrations, respectively (Deacon & Phillips, 1980; Nakamoto, 1986). The <sup>1</sup>H NMR spectra of ligands L1–L3 and complexes [C<sub>30</sub>H<sub>22</sub>N<sub>4</sub>O<sub>4</sub>S<sub>2</sub>Zn], [C<sub>30</sub>H<sub>20</sub>Cl<sub>2</sub>N<sub>4</sub>O<sub>4</sub>S<sub>2</sub>Zn] and [C<sub>30</sub>H<sub>20</sub>F<sub>2</sub>N<sub>5</sub>O<sub>7</sub>S<sub>2</sub>Zn] revealed signals in the range 6.90–7.99 ppm range assigned to aromatic protons. A singlet corresponding to the azomethine group was observed in the ~9.43–9.26 ppm range which was shifted to 8.13–8.17 ppm in the complexes suggesting coordination of the N-atom to the metal ion (Kalaivani et al., 2012). The ligands displayed singlets at ~12.44–11.12 ppm attributed to the OH group (Mandegani, Asadi, Asadi, Karbalaeei–Heidari & Rastegari, 2016) which was found absent in the spectra of complexes indicating coordination to Zn(II) metal ion upon deprotonation. In the <sup>13</sup>C NMR spectra, the azomethine carbon signatures were observed at 167.49–166.51 ppm which was shifted to 168.35–167.34 ppm in the complexes while aromatic carbon signatures were observed ~103.26–135.33 ppm (Fig.S2).

The ESI mass spectra of ligands L1–L3 exhibited molecular ion peak [M<sup>+</sup>] at  $m/z = 283, 318$  and  $303$ , corresponding to [C<sub>15</sub>H<sub>12</sub>N<sub>2</sub>O<sub>2</sub>S]<sup>+</sup>, [C<sub>15</sub>H<sub>11</sub>ClN<sub>2</sub>O<sub>2</sub>S]<sup>+</sup> and [C<sub>15</sub>H<sub>11</sub>FN<sub>2</sub>O<sub>2</sub>S]<sup>+</sup> moieties, respectively. The mass spectra of metal complexes **1** (a–c) showed  $m/z$  molecular ion peak at  $691.08, 758.75$  and  $730.77$ , corresponding to [C<sub>30</sub>H<sub>22</sub>CuN<sub>5</sub>O<sub>7</sub>S<sub>2</sub>]<sup>+</sup>, [C<sub>30</sub>H<sub>20</sub>Cl<sub>2</sub>CuN<sub>5</sub>O<sub>7</sub>S<sub>2</sub>]<sup>+</sup> and

$[\text{C}_{30}\text{H}_{20}\text{CuF}_2\text{N}_5\text{O}_7\text{S}_2]^+$  moieties. The mass spectra for complexes **2** (a–c) displayed molecular ion peaks at  $m/z = 632.11$ ,  $700.79$  and  $667.1$ , associated with  $[\text{C}_{30}\text{H}_{22}\text{N}_4\text{O}_4\text{S}_2\text{Zn}]^+$ ,  $[\text{C}_{30}\text{H}_{20}\text{Cl}_2\text{N}_4\text{O}_4\text{S}_2\text{Zn}]^+$  and  $[\text{C}_{30}\text{H}_{20}\text{F}_2\text{N}_5\text{O}_7\text{S}_2\text{Zn}]^+$  moieties, respectively. The spectra of metal complexes also displayed fragmentation peaks corresponding to their respective ligand moieties (Fig.S3)

To further deduce structural information, the electronic spectra of the complexes **1** and **2** (a–c) were measured in the UV–Vis region (200–700 nm). The electronic absorption spectra of the ligands displayed peaks at 260–264 and 348–341 nm corresponding to  $\pi$ – $\pi^*$  and low energy  $n$ – $\pi^*$  ligand centered (IL) transitions. However, these bands were shifted to 270–275 and 354–367 nm suggesting coordination of the ligand to Zn(II) ion in complexes  $[\text{C}_{30}\text{H}_{22}\text{N}_4\text{O}_4\text{S}_2\text{Zn}]$ ,  $[\text{C}_{30}\text{H}_{20}\text{Cl}_2\text{N}_4\text{O}_4\text{S}_2\text{Zn}]$  and  $[\text{C}_{30}\text{H}_{20}\text{F}_2\text{N}_5\text{O}_7\text{S}_2\text{Zn}]$ , respectively (Enamullah et al., 2016). The electronic spectra of complexes  $[\text{C}_{30}\text{H}_{22}\text{CuN}_5\text{O}_7\text{S}_2]$ ,  $[\text{C}_{30}\text{H}_{20}\text{Cl}_2\text{CuN}_5\text{O}_7\text{S}_2]$  and  $[\text{C}_{30}\text{H}_{20}\text{CuF}_2\text{N}_5\text{O}_7\text{S}_2]$  also showed low intensity broad bands centered at 521, 529 and 526 nm in the visible region attributed to  $d$ – $d$  transitions, consistent with the pentacoordinated geometry of the complexes (Bhowmik, Das, Chattopadhyay & Ghosh, 2015).

The magnetic susceptibility measurement of complexes  $[\text{C}_{30}\text{H}_{22}\text{CuN}_5\text{O}_7\text{S}_2]$ ,  $[\text{C}_{30}\text{H}_{20}\text{Cl}_2\text{CuN}_5\text{O}_7\text{S}_2]$  and  $[\text{C}_{30}\text{H}_{20}\text{CuF}_2\text{N}_5\text{O}_7\text{S}_2]$  were carried out at room temperature to provide insights into the geometry around the Cu(II) ion and to ascertain its paramagnetic nature. The observed magnetic moment value for complexes **1** (a–c) were found to be 1.75, 1.77 and 1.76 BM which is slightly higher than the spin only value due to one unpaired electron ( $\mu_{\text{eff}} = 1.73$  BM), suggesting a possible penta coordinated geometry (Latif & Mohamed 2018).

However, complexes  $[\text{C}_{30}\text{H}_{22}\text{N}_4\text{O}_4\text{S}_2\text{Zn}]$ ,  $[\text{C}_{30}\text{H}_{20}\text{Cl}_2\text{N}_4\text{O}_4\text{S}_2\text{Zn}]$  and  $[\text{C}_{30}\text{H}_{20}\text{F}_2\text{N}_5\text{O}_7\text{S}_2\text{Zn}]$  were

found to be diamagnetic in nature, consistent with the tetrahedral geometry, respectively (Orojloo, Mohamed, Zolgharnein, Solimannejad & Amani., 2017).

The solid state X-band EPR spectra of complexes  $[C_{30}H_{22}CuN_5O_7S_2]$ ,  $[C_{30}H_{20}Cl_2CuN_5O_7S_2]$  and  $[C_{30}H_{20}CuF_2N_5O_7S_2]$  were recorded at room temperature under the magnetic field strength  $3000 \pm 1000$  G using tetracyanoethylene as a field marker (Fig.S4). All the complexes **1** (a–c) displayed an isotropic EPR spectra exhibiting axial symmetry with  $g_{||} = 2.212$ ,  $g_{||} = 2.214$ ,  $g_{||} = 2.213$ ,  $g_{\perp} = 2.031$ ,  $g_{\perp} = 2.064$ ,  $g_{\perp} = 2.051$  and  $g_{av} = 2.10$ ,  $g_{av} = 2.12$ ,  $g_{av} = 2.11$ , respectively computed from the formula  $g_{av}^2 = g_{||}^2 + 2g_{\perp}^2/3$ . These parameters were consistent with the penta coordinated geometry of the copper(II) metal ion (Arruda et al., 2017). The  $g_{||} \leq 2.2$  is in agreement with the covalent character of the metal ligand bond (Kumar, Singh, Garg & Singh, 2003).

### 3.5. DNA binding studies

#### 3.5.1. Absorption titrations

Since benzothiazole is an important bioactive heterocyclic pharmacophore, its relevance in metallo-pharmaceuticals as a metal anchoring scaffold is enhanced by forming Schiff base with other ancillary ligands. The structure-activity relationship (SAR) of benzothiazoles *viz.*, unsubstituted, chloro and fluoro derivatives,  $[C_{30}H_{22}CuN_5O_7S_2]$ ,  $[C_{30}H_{20}Cl_2CuN_5O_7S_2]$ ,  $[C_{30}H_{20}CuF_2N_5O_7S_2]$ ,  $[C_{30}H_{22}N_4O_4S_2Zn]$ ,  $[C_{30}H_{20}Cl_2N_4O_4S_2Zn]$  and  $[C_{30}H_{20}F_2N_5O_7S_2Zn]$  with CT-DNA can lay a platform for the design of rational newer antitumor drug candidates. The binding propensity of complexes **1** and **2** (a–c) with CT-DNA was studied by carrying out absorption titrations with concomitant addition of CT-DNA ( $0.00$ – $5.5 \times 10^{-5}$  M). Strong interactions between the metal complexes and the DNA base pairs results in hypochromism in the absorption intensity with bathochromic shift due to stacking interactions of the aromatic moiety inside the DNA helix resulting in conformational changes. However, minor groove

binding interaction of the complexes with the DNA usually results in hyperchromism with no red/blue shift (Banerjee et al., 2018). An increase in the absorbance of the complexes **1** and **2** (a–c) was observed at 265 nm indicating “hyperchromic” effect and “hypochromic” shift was observed at the intraligand absorption band centered at 397 nm (Fig.2). These changes in the absorbance were attributed to groove binding mode of complexes with partial intercalation (Liu et al., 2018; Zhang et al., 2017). In order to quantify the binding strength the intrinsic binding constant,  $K_b$  values were obtained by using Wolfe–Shimer equation (1);

$$\frac{[DNA]}{\varepsilon_a - \varepsilon_f} = \frac{[DNA]}{\varepsilon_b - \varepsilon_f} + \frac{1}{K_b(\varepsilon_a - \varepsilon_f)} \quad (1)$$

where  $\varepsilon_a$ ,  $\varepsilon_f$  and  $\varepsilon_b$  are the apparent extinction coefficient ( $A_{obs}/[M]$ ), the extinction coefficient for free metal complex (M), and the extinction coefficient for the metal complex (M) in the fully bound form, respectively. The  $K_b$  values of complexes **1** and **2** (a–c) are found to be  $4.02(\pm 0.15) \times 10^5$ ,  $4.40(\pm 0.08) \times 10^5$ ,  $4.26(\pm 0.11) \times 10^5$ ,  $3.07(\pm 0.12) \times 10^5$ ,  $3.67(\pm 0.09) \times 10^5$  and  $3.31(\pm 0.12) \times 10^5 \text{ M}^{-1}$ , respectively.

The binding constant values suggested that Cu(II) complexes [ $C_{30}H_{22}CuN_5O_7S_2$ ], [ $C_{30}H_{20}Cl_2CuN_5O_7S_2$ ] and [ $C_{30}H_{20}CuF_2N_5O_7S_2$ ], demonstrated higher binding propensity for CT–DNA than corresponding zinc complexes [ $C_{30}H_{22}N_4O_4S_2Zn$ ], [ $C_{30}H_{20}Cl_2N_4O_4S_2Zn$ ] and [ $C_{30}H_{20}F_2N_5O_7S_2Zn$ ] and followed the trend **1b** > **1c** > **1a** > **2b** > **2c** > **2a** which was further substantiated by other spectroscopic studies. The rationale for higher binding strength of complexes is due to the presence of electron withdrawing group which increases  $\pi$ –stacking ability of the benzothiazole moiety and further induces positive charge for electrostatic interaction (Lu et al., 2008).

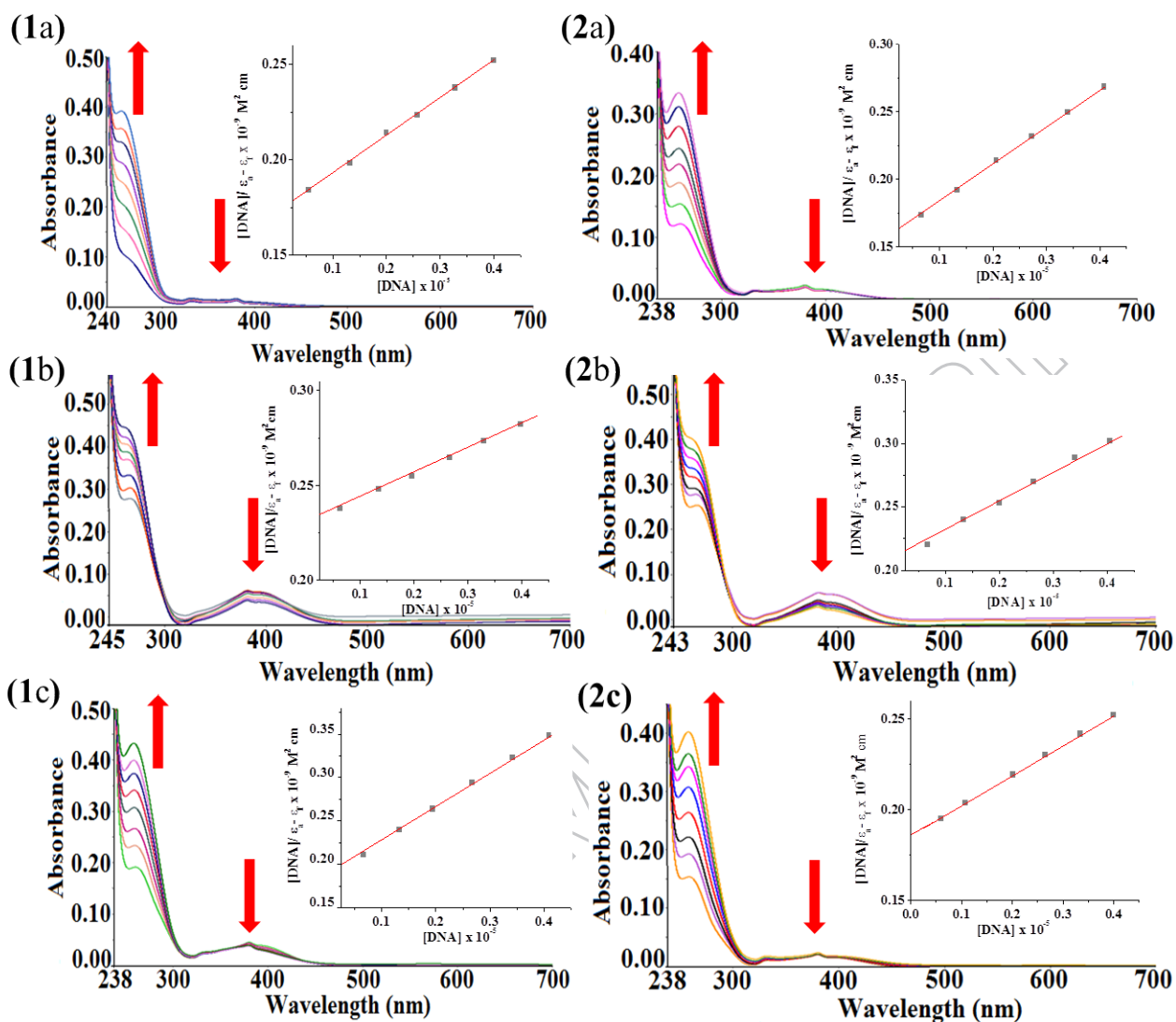


**Fig.2.** UV-vis titration spectra of complexes **1** and **2** (a-c) in presence of CT-DNA.

### 3.5.2. Fluorescence titrations

Another more sensitive optical fluorescence titration technique was employed to quantify the magnitude of binding of complexes **1** and **2** (a-c) corresponding to  $[C_{30}H_{22}CuN_5O_7S_2]$ ,  $[C_{30}H_{20}Cl_2CuN_5O_7S_2]$ ,  $[C_{30}H_{20}CuF_2N_5O_7S_2]$ ,  $[C_{30}H_{22}N_4O_4S_2Zn]$ ,  $[C_{30}H_{20}Cl_2N_4O_4S_2Zn]$  and  $[C_{30}H_{20}F_2N_5O_7S_2Zn]$ , respectively with CT-DNA. In the absence of CT-DNA, complexes **1** and **2** (a-c) emit strong luminescence (Fig.S5) with a maxima appearing at 290–310 nm (excited at 265 nm). There was an apparent increase in the fluorescence intensity upon

increasing concentration of CT–DNA which implicates strong interactions between complex and the DNA base pairs. The results showed that the increase in emission intensities upon binding to CT–DNA support strong interaction of complexes **1** and **2** (a–c) with CT–DNA (Chan, Ma, Yang & Che, 2003; Bhat, Kumbhar, Lönnecke & HeyHawkins, 2010). The binding strength of complexes **1** and **2** (a–c) were ascertained by the binding constant ( $K$ ) values derived from Scatchard equation (Cui et al., 2009) and was found to be  $3.09(\pm 0.03) \times 10^5$ ,  $3.21(\pm 0.19) \times 10^5$ ,  $3.11(\pm 0.08) \times 10^5$ ,  $2.01(\pm 0.11) \times 10^5$ ,  $2.25(\pm 0.06) \times 10^5$  and  $2.11(\pm 0.05) \times 10^5 \text{ M}^{-1}$ , respectively.

### 3.5.3. Competitive binding assay

In order to get further insight into the binding affinities of complexes competitive binding experiments were carried out on EB–DNA system by varying the concentration of the complex. EB is a planar cationic dye that emits intense fluorescence in presence of CT–DNA at *ca.* 600 nm ( $\lambda_{em}$ ) due to its strong intercalation between the adjacent base pairs. The enhanced fluorescence was quenched upon addition of the second molecule by replacing the bound EB or accepting the excited electron from EB.

Fluorescence quenching of the EB–DNA system in the presence of complexes  $[\text{C}_{30}\text{H}_{22}\text{CuN}_5\text{O}_7\text{S}_2]$ ,  $[\text{C}_{30}\text{H}_{20}\text{Cl}_2\text{CuN}_5\text{O}_7\text{S}_2]$ ,  $[\text{C}_{30}\text{H}_{20}\text{CuF}_2\text{N}_5\text{O}_7\text{S}_2]$ ,  $[\text{C}_{30}\text{H}_{22}\text{N}_4\text{O}_4\text{S}_2\text{Zn}]$ ,  $[\text{C}_{30}\text{H}_{20}\text{Cl}_2\text{N}_4\text{O}_4\text{S}_2\text{Zn}]$  and  $[\text{C}_{30}\text{H}_{20}\text{F}_2\text{N}_5\text{O}_7\text{S}_2\text{Zn}]$  was carried out to characterize the binding mode of these complexes (Fig. 3). Since EB was not completely displaced, partial intercalation mode of interaction cannot be ruled out (Gou et al., 2017). Furthermore, the extent of quenching was determined by using the Stern–Volmer equation and the  $K_{sv}$  value for complexes **1** and **2** (a–c) were found to be 2.21, 2.42, 2.22, 1.12, 1.54, and 1.28 respectively.

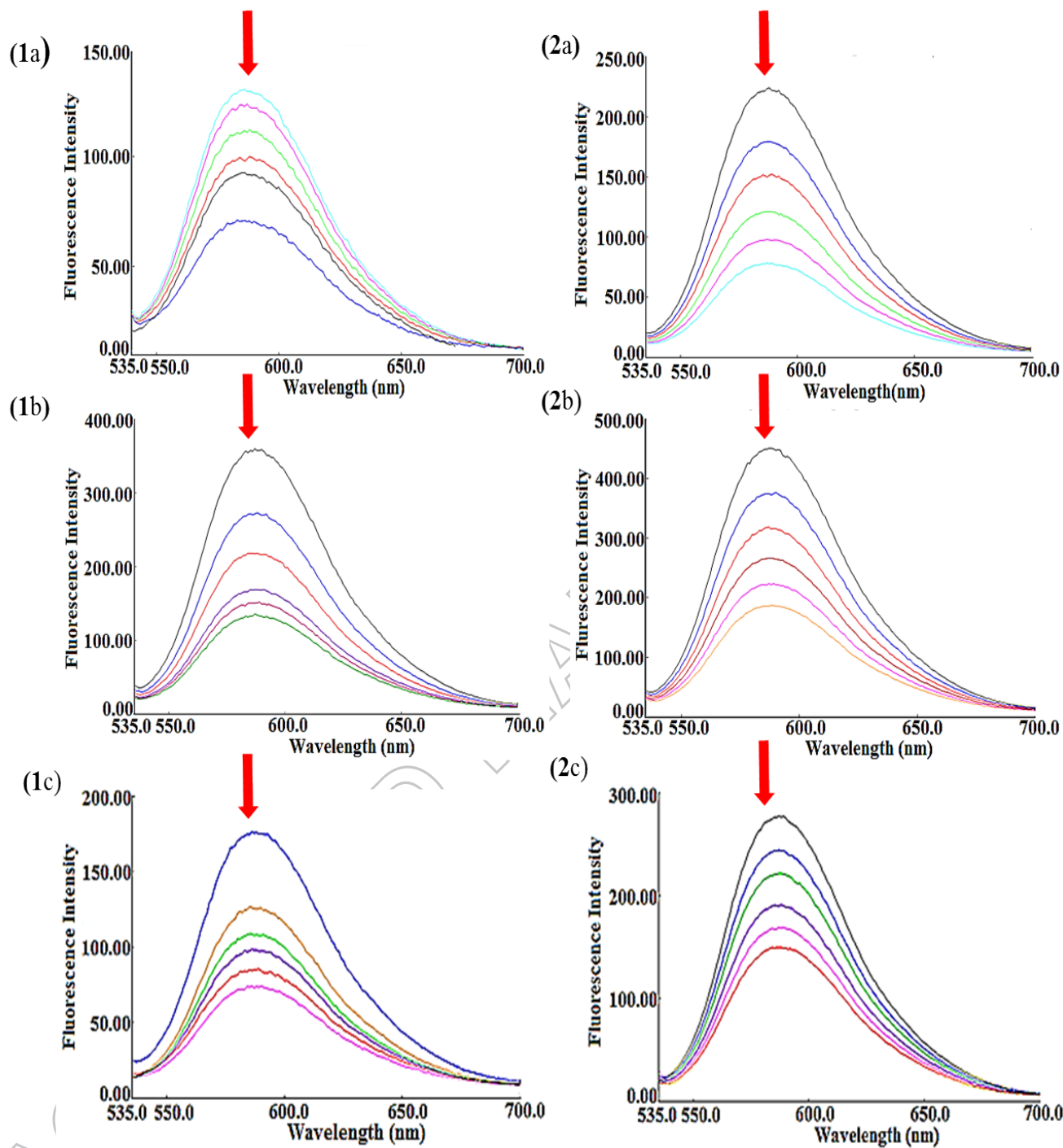


**Fig.3.** Emission titration spectra of the EB- CT-DNA system of complexes **1** and **2** (a-c).

To validate the groove binding preference of the complexes **1** and **2** (a-c) fluorescence

competitive binding studies were carried out by employing DAPI

(4',6-diamidino-2-phenylindole) as an external fluorophore. DAPI is a minor groove binding

fluorescent dye that binds preferentially in the AT-rich regions of B-DNA (Larsen, Goodsell, Cascio, Grzeskowiak & Dickerson, 1989; Trotta & Paci, 1998; Banerjee & Pal, 2008). Upon binding to CT-DNA, 1:1 complex of DNA and dye exhibited an enhancement in the emission maxima ( $\lambda_{ex} = 358 \text{ nm}$ ,  $\lambda_{em} = 461 \text{ nm}$ ). In the groove binder displacement assay a significant decrease was observed upon concomitant addition of metal complexes  $[\text{C}_{30}\text{H}_{22}\text{CuN}_5\text{O}_7\text{S}_2]$ ,  $[\text{C}_{30}\text{H}_{20}\text{Cl}_2\text{CuN}_5\text{O}_7\text{S}_2]$ ,  $[\text{C}_{30}\text{H}_{20}\text{CuF}_2\text{N}_5\text{O}_7\text{S}_2]$ ,  $[\text{C}_{30}\text{H}_{22}\text{N}_4\text{O}_4\text{S}_2\text{Zn}]$ ,  $[\text{C}_{30}\text{H}_{20}\text{Cl}_2\text{N}_4\text{O}_4\text{S}_2\text{Zn}]$  and  $[\text{C}_{30}\text{H}_{20}\text{F}_2\text{N}_5\text{O}_7\text{S}_2\text{Zn}]$  to the DAPI-DNA system (Fig. 4). The observed decrease in fluorescence intensity is suggestive of the gradual displacement of the DAPI by the metal complexes, indicative of the preferential groove binding mode of the complexes (Yun et al., 2003). The quantitative determination of the extent of quenching was done by employing Stern Volmer equation to calculate the quenching constants for the complexes 1 and 2 (a-c) and were found to be 2.54, 2.95, 2.76, 1.56, 1.89, and 1.62, respectively.

**Table.1.** Intrinsic binding constant  $K_b$ , Binding constant  $K$  and Stern – Volmer quenching constant  $K_{sv}$  values for the complexes **1** and **2** (a-c) with CT-DNA.

Complexes	$K_b (\text{M}^{-1})$	$K (\text{M}^{-1})$	$K_{sv}$
1a	$4.02(\pm 0.15) \times 10^5$	$3.09(\pm 0.03) \times 10^5$	2.21
1b	$4.40(\pm 0.08) \times 10^5$	$3.21(\pm 0.19) \times 10^5$	2.42
1c	$4.26(\pm 0.11) \times 10^5$	$3.11(\pm 0.08) \times 10^5$	2.22
2a	$3.07(\pm 0.12) \times 10^5$	$2.01(\pm 0.11) \times 10^5$	1.12
2b	$3.67(\pm 0.09) \times 10^5$	$2.25(\pm 0.06) \times 10^5$	1.54
2c	$3.31(\pm 0.12) \times 10^5$	$2.11(\pm 0.05) \times 10^5$	1.28

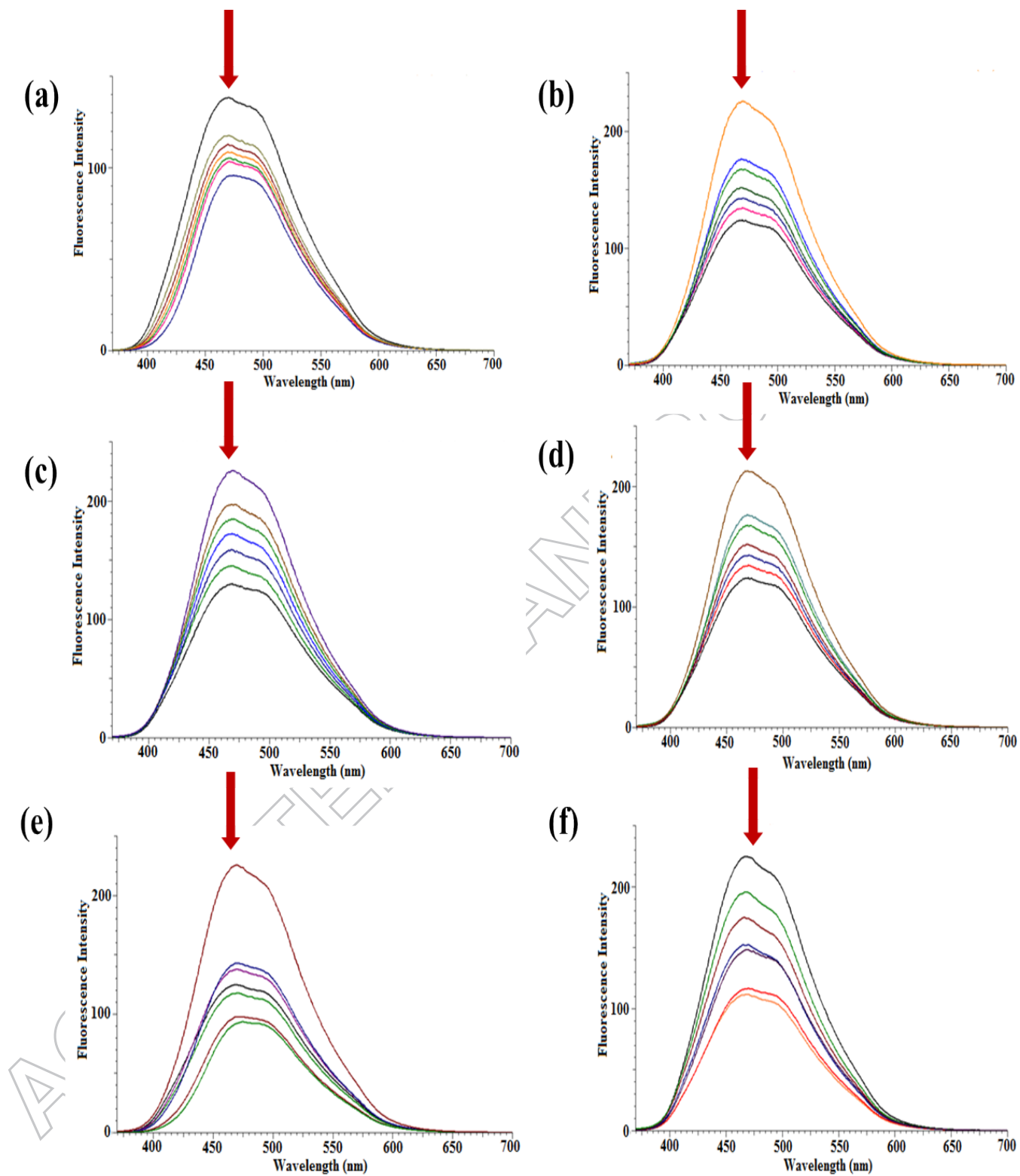


**Fig.4.** Emission titration spectra of the DAPI- CT-DNA system of complexes 1 and 2 (a-c).

### 3.5.4. Hydrodynamic measurements

To further investigate the binding mode between the complexes **1** and **2** (a–c) with CT–DNA, hydrodynamic measurements were carried out. Intercalation results in the lengthening of the DNA helix, leading to an increase in the DNA viscosity. In contrast, complexes that binds exclusively in DNA grooves by partial or non–classical intercalation may bend or kink DNA helix, causing less pronounced (positive or negative) change in the effective length of DNA thereby decreasing its viscosity (Satyanarayana, Dabrowiak & Chaires, 1993). The effect of each complex on the viscosity of CT–DNA was investigated in order to assess the binding mode and strength of these complexes. The plots of  $(\eta/\eta_0)^{1/3}$  vs R (where  $R = [\text{complex}]/[\text{DNA}]$ ;  $\eta$  and  $\eta_0$  are the relative viscosities of CT–DNA in presence and absence of complexes, respectively) gives a measure of the viscosity changes (Fig. 5). In our experiments it was observed that the complexes  $[\text{C}_{30}\text{H}_{22}\text{CuN}_5\text{O}_7\text{S}_2]$ ,  $[\text{C}_{30}\text{H}_{20}\text{Cl}_2\text{CuN}_5\text{O}_7\text{S}_2]$ ,  $[\text{C}_{30}\text{H}_{20}\text{CuF}_2\text{N}_5\text{O}_7\text{S}_2]$ ,  $[\text{C}_{30}\text{H}_{22}\text{N}_4\text{O}_4\text{S}_2\text{Zn}]$ ,  $[\text{C}_{30}\text{H}_{20}\text{Cl}_2\text{N}_4\text{O}_4\text{S}_2\text{Zn}]$  and  $[\text{C}_{30}\text{H}_{20}\text{F}_2\text{N}_5\text{O}_7\text{S}_2\text{Zn}]$  exhibited a decrease in the relative viscosity of CT–DNA and follows the trend  $1b > 1c > 1a > 2b > 2c > 2a$ . Moreover, the results of hydrodynamic measurements are in close concordance with other biophysical studies and support the groove binding mode of the complexes (Lakshmi Prabaa et al., 2015; Arif et al., 2018).

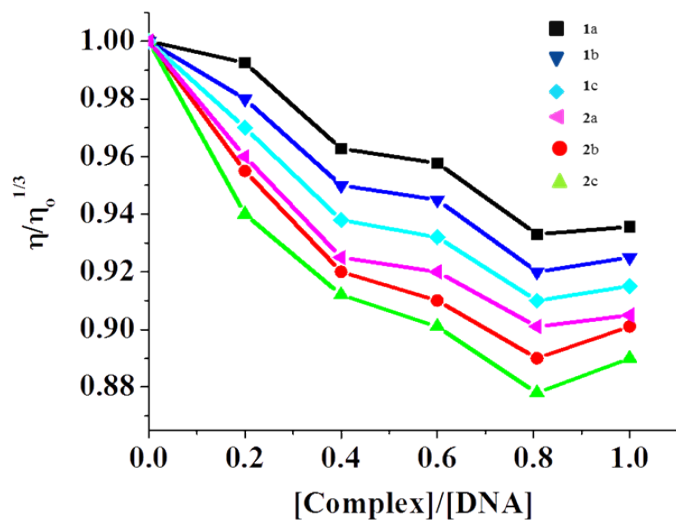


**Fig. 5.** Effect of complexes **1** and **2** (a–c) on the relative viscosities ( $\eta/\eta_0$ ) of CT–DNA.

### 3.6. Structure–activity relationship (SAR) studies

To rationalize the DNA binding constants and to analyze the drug–likeness of the complexes, structure–activity relationship (SAR) studies were carried out. There are several basic features which affect a molecule to be a drug, and they are described as a ‘‘Lipinski’s rule of five’’: (i) Log P should not exceed 5; (ii) Molecular weight not exceeding 500 Da; (iii) Number of hydrogen bond acceptors not exceeding 10; (iv) Number of hydrogen bond donors not exceeding 5 (Maass, Schulz–Gasch, Stahl & Rarey 2007). Various molecular properties (TPSA, miLogP, molecular weight, OH–NH interaction, O–N interaction, nrotb and number violations from Lipinski rule) are calculated using molinspiration software (Table 2). Topological polar surface area (TPSA) and lipophilicity (LogP) are two important parameters for predicting oral bioavailability of drug molecules (Parvez et al., 2010; Jarrahpour et al., 2012). Molecules having TPSA value of 140 Å<sup>2</sup> or more are expected to show poor absorption (Veber et al., 2002).

Molinspiration calculations for the ligands indicated that all the compounds have TPSA values < 140 Å<sup>2</sup> and they are expected to have good intestinal absorption. As the cytotoxicity of

anticancer agents is linked with their ability to accumulate within the cells, lipophilicity plays a major role in their bioactivity. In general, more the lipophilicity of the ligand more will be its potency to act as cytotoxic agent when coordinated to the metal centre and vice versa. The results have shown that chloro derived ligand, L2 was found to be more lipophilic which is responsible for its better uptake in the cell membranes. This is also evidenced in the chloro substituted synthesized complex  $[C_{30}H_{20}Cl_2CuN_5O_7S_2]$ , which has demonstrated higher binding affinity with CT-DNA and good cytotoxic activity as compared to other complexes. None of the ligand skeletons L1–L3 (Fig.6) tested showed violation of drug-likeness rule.

**Table.2.** Molinspiration calculated properties of substituted benzothiazole derived ligands L1–L3.

Properties	L1	L2	L3
miLogP	3.57	4.20	3.71
TPSA	54.72	54.72	54.72
n atoms	20	21	21
MW	284.24	318.79	302.22
nON	4	4	4
nOHNH	1	1	1
n violations	0	0	0
nrotb	3	3	3
Volume	242.82	256.26	247.75

miLogP – theoretically calculated Log P; TPSA – Total Polar Surface Area; MW – Molecular Weight; nON – number of hydrogen bond acceptors; nOHNH – number of hydrogen bond donors; n violations – number of violated drug-likeness rules; nrotb – number of rotating bonds, Volume – molecular volume.

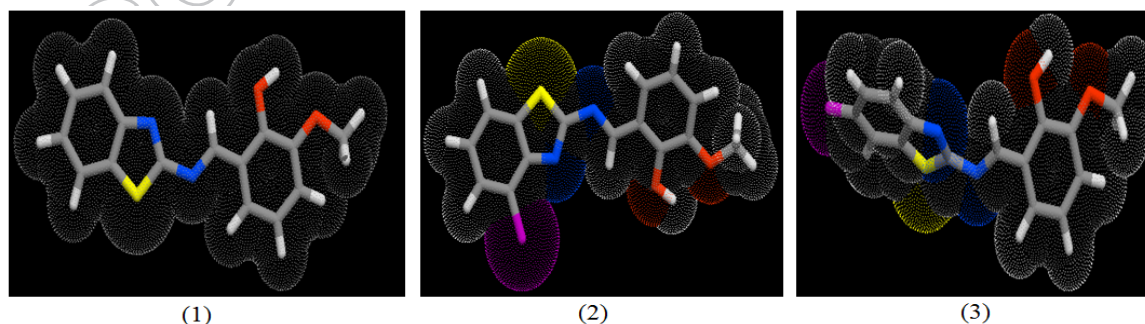


**Fig.6.** Molinspiration generated 3D structure of substituted benzothiazole derived ligands L1–L3.

### 3.7. Antimicrobial activity

To overcome the resistance due to microbial infections, Schiff base derived transition metal complexes are developed to evaluate their efficient bioactivity against various pathogens. The ligands L1–L3 and their complexes **1** and **2** (a–c) were screened for the *in vitro* antibacterial activity against Gram–positive *B. subtilis*, *S. aureus* and Gram–negative *E. coli*, *P. aeruginosa*, and *in vitro* antifungal activity against *C. albicans* and the relevant data are presented in Table 3. The antibacterial activity of ligands L1–L3 and their complexes  $[C_{30}H_{22}CuN_5O_7S_2]$ ,  $[C_{30}H_{20}Cl_2CuN_5O_7S_2]$ ,  $[C_{30}H_{20}CuF_2N_5O_7S_2]$ ,  $[C_{30}H_{22}N_4O_4S_2Zn]$ ,  $[C_{30}H_{20}Cl_2N_4O_4S_2Zn]$  and  $[C_{30}H_{20}F_2N_5O_7S_2Zn]$  were evaluated by measuring the diameter of the zone of inhibition (mm) to compare with the commercial drug (doxycycline). A comparative study indicates that metal complexes exhibit higher antibacterial and antifungal activity than the parent Schiff base ligands (Fig.7). It has been reported previously in the literature that the bioactivity of a ligand is enhanced upon metal complexation which can be explained on the basis of Overtone's concept and Chelation theory (Joseph, Nagashri & Janaki, 2012). In case of transition metal complexes, chelation considerably reduces the polarity of the metal ion due to (a) overlap of ligand orbital, (b) partial sharing of positive charge with donor groups and (c) possible  $\pi$ –electron delocalization over the entire chelate ring. Such chelation increases the lipophilic character of the complexes, thereby favouring easy penetration into the lipid membrane and inhibiting the growth of the microorganisms (Khosravi & Torshizi, 2018).

The complexes  $[C_{30}H_{20}Cl_2CuN_5O_7S_2]$  and  $[C_{30}H_{20}Cl_2N_4O_4S_2Zn]$ , showed maximum zone of inhibition, 23 and 21 mm against Gram–negative *E. coli* as compared to the positive control, doxycycline (19mm). The complexes also showed remarkably good anti–bacterial activity against *S. aureus* while moderate activity against *B. subtilis* and *P. aeruginosa*. The synthesized

complexes were also screened for their antifungal activity against *C. albicans* exhibiting promising antifungal activities with a broad spectrum effect. The complexes  $[C_{30}H_{20}Cl_2CuN_5O_7S_2]$  and  $[C_{30}H_{20}Cl_2N_4O_4S_2Zn]$ , exhibited prominent antifungal activity against the *C. albicans* with zone diameter of 27 and 25 mm, respectively. The screening results indicated that complexes  $[C_{30}H_{20}Cl_2CuN_5O_7S_2]$  and  $[C_{30}H_{20}Cl_2N_4O_4S_2Zn]$  exhibited promising activity against these pathogens as compared with other metal complexes. The disparity observed in the activity of complexes against different microorganisms depends upon the nature of the metal ions, their coordination modes and impermeability in the microbial cells.

**Table.3.** *In vitro* antimicrobial activity of ligands L1–L3 and complexes 1 and 2 (a–c). Complexes =1000 µg/ml, Doxycycline 30 µg/disc, --- No zone of inhibition, NA = Not defined

Complexes	Zone of inhibition (mm)				
	<i>B. subtilis</i>	<i>S. aureus</i>	<i>E. coli</i>	<i>P. aeruginosa</i>	<i>C. albicans</i>
L1	---	11±0.57	11±1.08	---	11±1.00
L2	---	15±0.67	14±.90	---	13±0.67
L3	12±0.33	13±1.00	14±0.50	---	12±0.80
1a	---	12±1.33	13±1.00	---	16±1.00
1b	17±1.15	21±2.01	23±2.18	15±0.90	27±2.09
1c	15±0.86	19±1.76	20±1.21	14±1.12	24±1.5
2a	---	11±1.33	---	---	14±0.33
2b	16±1.01	20±1.08	21±1.9	14±1.01	25±1.78
2c	14±0.91	17±1.91	18±2.03	14±0.50	23±1.00
<b>Positive Control (Dx)</b>	22±2.90	22±2.12	19±1.25	NA	----

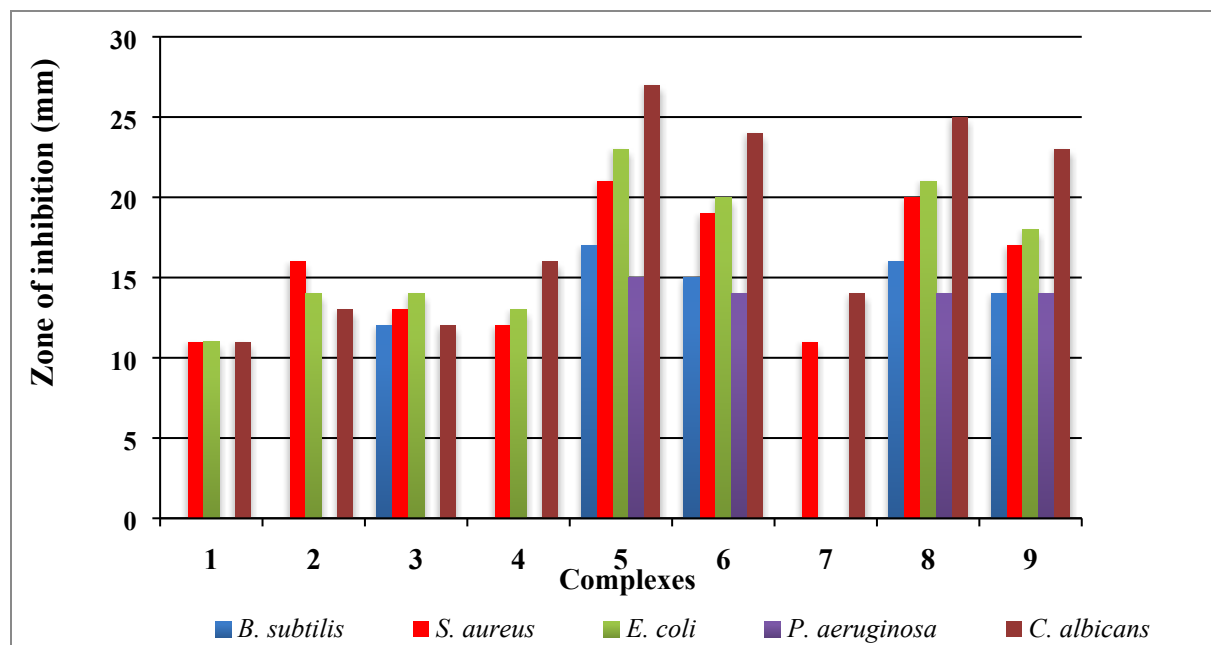


**Fig.7.** The antimicrobial activity of ligands L1–L3 and complexes 1 and 2 (a–c).

### 3.8. *In vitro* cytotoxic assay

*In vitro* cytotoxicity of benzothiazole–derived chemotherapeutic agents 1 and 2 (b & c) viz.,  $[C_{30}H_{20}Cl_2CuN_5O_7S_2]$ ,  $[C_{30}H_{20}CuF_2N_5O_7S_2]$ ,  $[C_{30}H_{20}Cl_2N_4O_4S_2Zn]$  and  $[C_{30}H_{20}F_2N_5O_7S_2Zn]$  were evaluated on five different human cancer cell lines viz., MCF–7 (breast), MIA–PA–CA–2 (pancreatic), HeLa (cervix) and Hep–G2 (Hepatoma) and A498 (Kidney) by SRB assay (Fig.8). The cytotoxic activity was evaluated in terms of  $GI_{50}$  (concentration of drug that produces 50% inhibition of the cell growth), TGI (concentration of the drug that produces total inhibition of the cell growth) and  $LC_{50}$  (concentration of the drug that kills 50% of the cell kill) values in  $\mu\text{g/ml}$  (Table 4 and S1). Comparing the cytotoxic potential of these antitumor drug entities, it was found that chloro substituted copper complex  $[C_{30}H_{20}Cl_2CuN_5O_7S_2]$ , exhibited pronounced cytotoxicity only against HeLa (cervix) cell line which was evidenced from its surprisingly low  $GI_{50}$  value of  $4.8 \mu\text{g/ml}$  as compared to the standard drug Adriamycin ( $GI_{50} < 10$ ).

**Table.4.** Cytotoxic activity of the complexes **1** and **2** (b & c) (in  $\mu\text{g/mL}$ ).  $\text{GI}_{50}$  = Concentration of drug producing a 50% inhibition of cell growth.

Complexes	$\text{GI}_{50}$ values ( $\mu\text{g/ml}$ )				
	MCF-7	MIA-PA-CA-2	HeLa	Hep-G2	A498
<b>1b</b>	31.2	31.2	4.8	59.2	61.7
<b>2b</b>	>80	49.38	<80	>80	49.38
<b>1c</b>	46.6	55.2	32.6	74.2	70.3
<b>2c</b>	24.5	48.2	58.3	>80	58.0

The cytotoxicity profile of complexes reveals the preferential selective nature of complexes against different cancer lines with moderate to high  $\text{GI}_{50}$  values. However, complex  $[\text{C}_{30}\text{H}_{20}\text{Cl}_2\text{CuN}_5\text{O}_7\text{S}_2]$ , was selective for HeLa cell line while its zinc analogue was inactive ( $\text{GI}_{50}$  value > 80) for the identical cell line. From these studies, it can be inferred that chloro substituted complex  $[\text{C}_{30}\text{H}_{20}\text{Cl}_2\text{CuN}_5\text{O}_7\text{S}_2]$ , is a potent antitumor drug entity which is quite in agreement with previous literature reports on cytotoxic effect of chloro substituted copper (II) Schiff base complexes (Qiao et al., 2011).

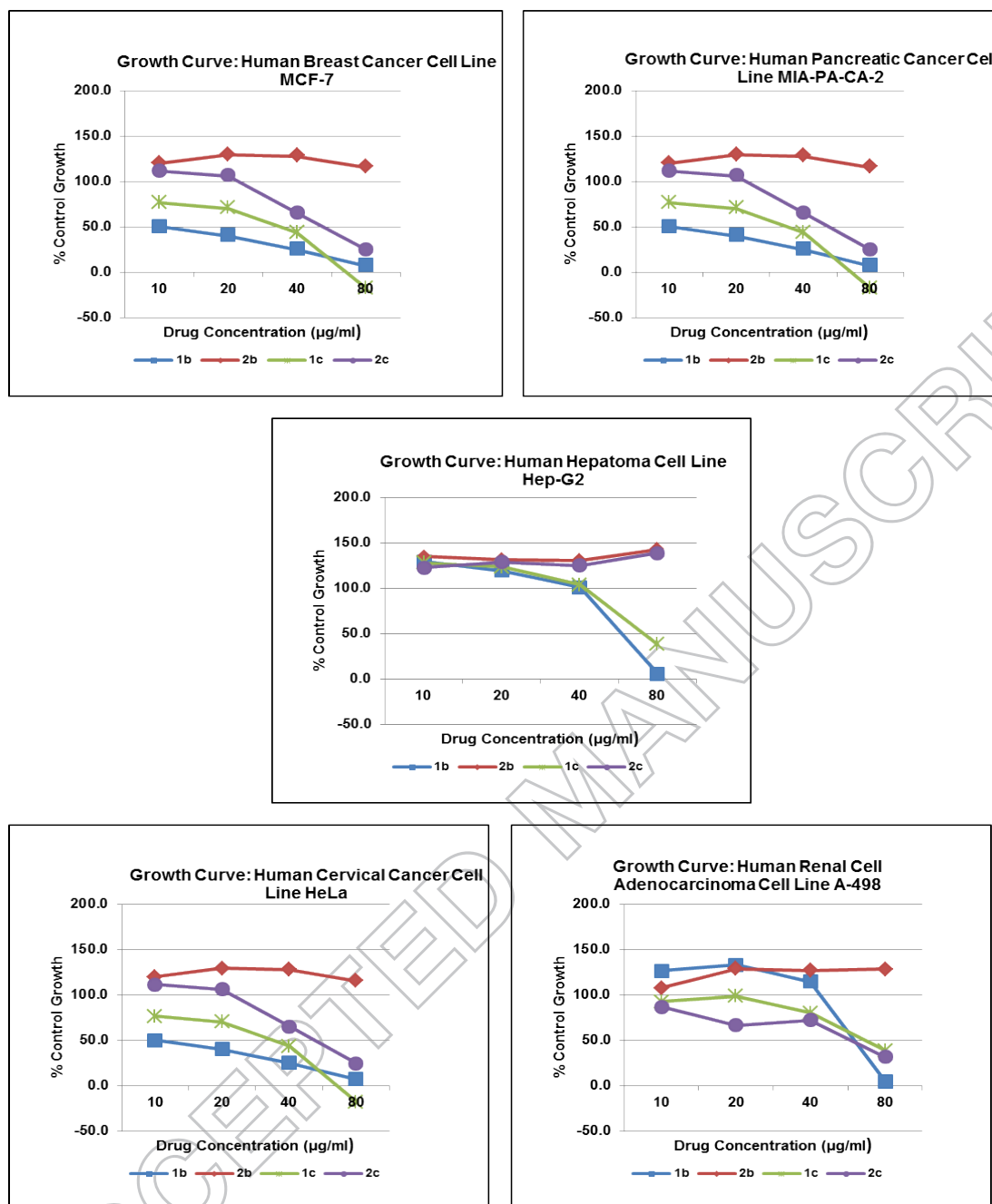


**Fig.8.** Growth curves showing % control growth vs. drug concentration ( $\mu\text{g/ml}$ ) against different human cancer cell lines.

### 3.9. Molecular docking studies

Molecular docking studies were performed with DNA duplex of sequence  $d(\text{CGCGAATTCGCG})_2$  dodecamer (PDB ID: 1BNA) in order to envisage the potential binding mode of the complexes inside the DNA helix thereby, validating our spectroscopic studies

(Zheng et al., 2014). The resulting docked model (Fig. 9 and S6) revealed that the complexes  $[C_{30}H_{22}CuN_5O_7S_2]$ ,  $[C_{30}H_{20}Cl_2CuN_5O_7S_2]$ ,  $[C_{30}H_{20}CuF_2N_5O_7S_2]$ ,  $[C_{30}H_{22}N_4O_4S_2Zn]$ ,  $[C_{30}H_{20}Cl_2N_4O_4S_2Zn]$  and  $[C_{30}H_{20}F_2N_5O_7S_2Zn]$  recognize the minor groove of the DNA within narrower G–C regions. The benzothiazole moiety extends into the DNA helix and interacts through hydrophobic and van der Waals interactions. The docked poses revealed significant  $\pi$ – $\pi$  stacking interactions and intricate hydrogen–bonding interactions between the –NH hydrogen of benzothiazole and the DNA base pairs which play a major role in stability of DNA complex adduct. The resulting binding energy calculated for the complexes **1** and **2** (a–c) was found to be –339, –372, –349, –324, –327, –325 KJ/mol, respectively. The relative lower binding energy of complex  $[C_{30}H_{20}Cl_2CuN_5O_7S_2]$ , indicates its strong binding affinity towards DNA helix consistent with the binding studies as well as the cytotoxicity results.

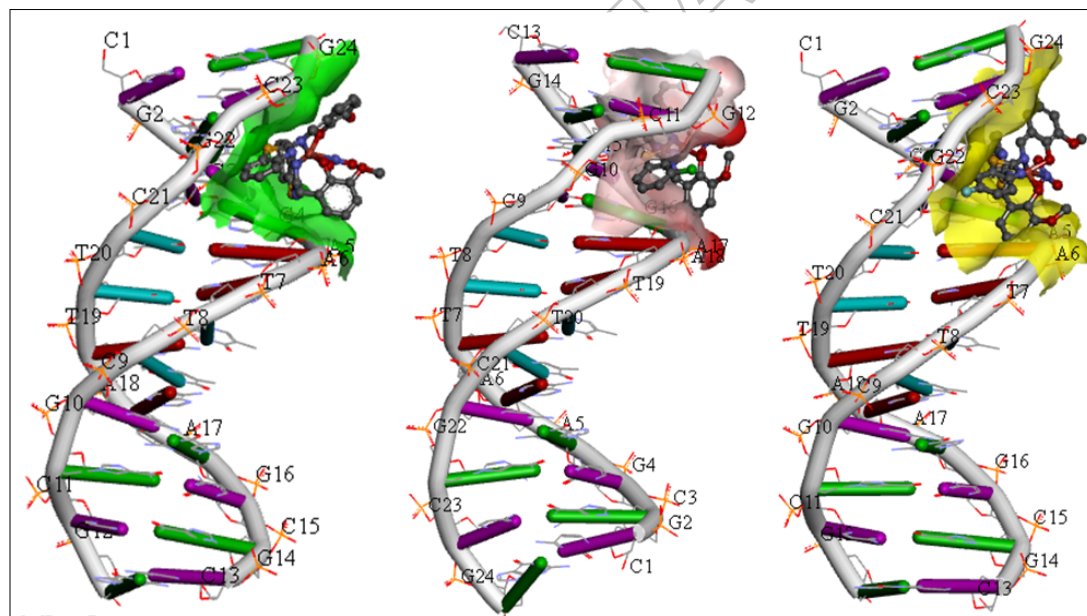


**Fig.9.** Molecular docked model of complexes **1**(a–c) illustrating minor groove preference in the GC region.

#### 4. Conclusion

New substituted benzothiazole Schiff base ligands and their Cu(II)/Zn(II) complexes endowed with efficient antimicrobial and anticancer properties have been synthesized and characterized by various spectroscopic techniques (FT-IR, EPR, NMR, ESI-MS) and elemental analysis. *In vitro* DNA-binding profile of the complexes **1** and **2** (a-c) were carried out by employing various biophysical methods which revealed groove mode of interaction with partial intercalation. The binding propensity was assessed by quantitative measurements which demonstrated higher binding of chloro-substituted complexes evidenced from their  $K_b$  and  $K_{sv}$  values. Structure-activity relationship (SAR) studies were carried out to investigate the effect of substituents on the molecular properties of the ligands and their metal complexes. The cytotoxic potential of substituted benzothiazole-derived anticancer drug entities was evaluated against various cancer cell lines. The cytotoxicity profile indicated that chloro substituted copper complex [C<sub>30</sub>H<sub>20</sub>Cl<sub>2</sub>CuN<sub>5</sub>O<sub>7</sub>S<sub>2</sub>] was found to be most active with a remarkably low IC<sub>50</sub> value of 4.8 µg/ml against HeLa cancer cell line compared to other analogues. Antimicrobial potential of substituted benzothiazole Schiff base ligands and metal complexes was evaluated against both the bacterial and fungal pathogens. The screening data reveals high antibacterial and antifungal activity of chloro substituted Cu(II) and Zn(II) complexes against *E.coli* and *C.albicans* in comparison with Doxycycline as standard drug with maximum zone of inhibition in the range of 27-21 mm. These results suggested that introduction of the electron withdrawing substituents into hetero-aromatic core is expected to increase the hydrophobic character and lipophilicity resulting in substantial biological activity of the complexes. In conclusion, our results demonstrated that the chloro substituted copper complexes display promising biological activities and can be developed as a potential antimicrobial and chemotherapeutic agent.

## Acknowledgments

The authors are grateful to SAIF Panjab University, Chandigarh, for providing elemental analysis, ESI–MS and NMR facilities. We are also thankful to Department of Chemistry, Aligarh Muslim University for providing the FT–IR, UV–vis, and EPR facility. The author (Sifteen Zehra) sincerely acknowledges financial support from University Grants Commission (UGC), New Delhi, for providing the fellowship and the Department of Chemistry, AMU through UGC assisted DRS–SAP, DST–FIST and DST PURSE Programme. The authors are highly thankful to Anticancer Drug screening facility (ACDSF) of ACTREC, Tata Memorial Centre, Navi Mumbai for carrying out in vitro anti–cancer activity of complexes by SRB assay.

## References

- Amiri, M., Ajloo, D., Fazli, M., Mokhtarieh, A., Grivani, G., & Saboury, A.A. (2017). Spectroscopic electrochemical, docking and molecular dynamics studies on the interaction of three oxovanadium (IV) Schiff base complexes with bovine serum albumin and their cytotoxicity against cancer. *Journal of Biomolecular Structure and Dynamics*. doi:10.1080/07391102.2017.1400467
- Arif, R., Nayab, P. S., Ansari, I. A., Shahid, M., Irfan, M., Alam, S., Abid, M., & Rahisuddin. (2018). Synthesis, molecular docking and DNA binding studies of phthalimide–based copper(II) complex: *In vitro* antibacterial, hemolytic and antioxidant assessment. *Journal of Molecular Structure*, 1160, 142–153. doi:10.1016/j.molstruc.2018.02.008
- Arjmand, F., Muddassir, M., Zaidi, Y., & Ray, D. (2013). Design, synthesis and crystal structure determination of dinuclear copper–based potential chemotherapeutic drug entities; *in vitro* DNA binding, cleavage studies and an evaluation of genotoxicity by micro nucleus test and comet assay. *Medicinal Chemistry Communications*, 4, 394–405. doi:10.1039/C2MD20141K

- Arruda, E. G. R. de., Farias, M. A. de., Jannuzzi, S. A. V., Gonsale, S. de A., Timm, R. A., Sharma, S.,..... & Formiga, A. L. B. (2017). Synthesis, Structural and magnetic characterization of a copper(II) complex of 2,6-di(1H-imidazol-2-yl) pyridine and its application in copper-mediated polymerization catalysis. *Inorganica Chimica Acta*, 466, 456–463. doi:10.1016/j.ica.2017.06.073
- Banerjee, D., & Pal, S.K.(2008). Dynamics in the DNA Recognition by DAPI: Exploration of the Various Binding Modes. *Journal of Physical Chemistry B*, 112, 1016–1021. doi:10.1021/jp077090f
- Banerjee, S., Ghorai, P., Brandão, P., Ghosh, D., Bhuiya, S., Chattopadhyay, D., Das, S., & Saha A. (2018). Syntheses, Crystal structures, DNA Binding, DNA cleavage, Molecular docking and DFT study of Cu(II) Complexes involving N<sub>2</sub>O<sub>2</sub> Donor azo Schiff Base Ligands. *New Journal of Chemistry*. doi:10.1039/C7NJ03293E
- Bhat, S. S., Kumbhar, A. S., Lönnecke P., & Hey Hawkins E. (2010). Self-Association of Ruthenium(II) Polypyridyl Complexes and Their Interactions with Calf Thymus DNA. *Inorganic Chemistry*, 49, 4843–4853. doi:10.1021/ic902374t
- Bhowmik, P., Das, L. K., Bauzá, A., Chattopadhyay, S., Frontera, A., & Ghosh, A. (2016). Anion dependent supramolecular architectures in Cu(II) complexes containing N<sub>2</sub>O-donor Schiff-base and 4,4'-bipyridine ligands: Structural analyses and theoretical studies. *Inorganica Chimica Acta*, 448, 26–33. doi:10.1016/j.ica.2016.03.049
- Bhowmik, P., Das, L.K., Chattopadhyaya, S., & Ghosh, A. (2015). A dinuclear and a 1D zigzag chain of copper(II) complexes with N<sub>2</sub>O donor Schiff base ligand and pseudohalides (azide and dicyanamide): Studies on catecholase-like activity. *Inorganica Chimica Acta*,

430, 24–29. doi:10.1016/j.ica.2015.01.039

Biswas, A., Das, L.K., Drew, M.G.B., Aromí, G., Gamez, P., & Ghosh, A., (2012). Synthesis, Crystal Structures, Magnetic Properties and Catecholase Activity of Double Phenoxido-Bridged. Penta-Coordinated Dinuclear Nickel(II) Complexes Derived from Reduced Schiff-Base Ligands: Mechanistic Inference of Catecholase Activity. *Inorganic Chemistry*, 51, 7993–8001. doi:10.1021/ic202748m

Creaven, B.S., Duff, B., Egan, D. A., Kavanagh, K., Rosair, G., Thangella, V. R., & Walsh, M. (2010). Anticancer and antifungal activity of copper(II) complexes of quinolin-2(1H)-one-derived Schiff bases. *Inorganica Chimica Acta*, 363, 4048–4058. doi:10.1016/j.ica.2010.08.009

Chan, L., Ma, D.L., Yang, M., & Che, C.M. (2003). Bis-intercalative dinuclear platinum(II) 6-phenyl-2,2'-bipyridine complexes exhibit enhanced DNA affinity but similar cytotoxicity compared to the mononuclear unit. *Journal of Biological Inorganic Chemistry*, 8, 761–769. doi:10.1007/s00775-003-0477-0

Cui, F., Yan, Y., Zhang, Q., Du, J., Yao, X., Qu, G., & Lu, Y. (2009). Characterization of the interaction between 2'-deoxyuridine and human serum albumin. *Carbohydrate Research*, 344, 642–647. doi:10.1016/j.carres.2009.01.009

Daravath, S., Kumar, M. P., Rambabu, A., Vamsikrishna, N., Ganji, N., & Shivaraj (2017). Design, synthesis, spectral characterization, DNA interaction and biological activity studies of copper(II), cobalt(II) and nickel(II) complexes of 6-amino benzothiazole derivatives. *Journal of Molecular Structure*, 1144, 147–158. doi:10.1016/j.molstruc.2017.05.022

Deacon, G., & Phillips, R. (1980). Relationships between the carbon-oxygen stretching

frequencies of carboxylato complexes and the type of carboxylate coordination.

*Coordination Chemistry Reviews*, 33, 227–250. doi:10.1016/S0010–8545(00)80455–5

Dehkhodaeia, M., Sahihia, M., & Rudbari, H. A. (2017). Spectroscopic and molecular docking studies on the interaction of Pd(II) & Co(II) Schiff base complexes with  $\beta$ -lactoglobulin as a carrier protein. *Journal of Biomolecular Structure and Dynamics*.

doi:10.1080/07391102.2017.1380537.

Enamullah, M., Makhloufi, G., Ahmed, R., Joy, B.A., Islam, M. A., Padula, D., & Janiak, C. (2016). Synthesis, X-ray, and Spectroscopic Study of Dissymmetric Tetrahedral Zinc(II) Complexes from Chiral Schiff Base Naphthaldiminate Ligands with Apparent Exception to the ECD Exciton Chirality. *Inorganic Chemistry*, 55, 6449–6464.

doi:10.1021/acs.inorgchem.6b00403

Facchinetti, V., Reis, R.R.da., Gomes, C.R.B., & Vasconcelos, T.R.A. (2012). Chemistry and biological activities of 1,3-benzothiazoles. *Mini Reviews in Organic Chemistry*, 9, 44–53. doi:10.2174/157019312799079929

Galindo–Murillo, R., García–Ramos, J. C., Ruiz–Azua, L., III Cheatham, T. E., & Cortés–Guzmán, F. (2015). Intercalation processes of copper complexes in DNA. *Nucleic Acids Research*, 43, 5364–5376. doi:10.1093/nar/gkv467

Gama, S., Rodrigues, I., Marques, F., Palma, E., Correia, I., Carvalho, M.F.N.N., & Paulo, A. (2014). New ternary bipyridine–terpyridine copper(II) complexes as self-activating chemical nucleases. *RSC Advances*, 4, 61363–61377. doi: 10.1039/C4RA12085J

Geary, W.J. (1971). The use of conductivity measurements in organic solvents for the characterization of coordination compounds. *Coordination Chemistry Reviews*, 7, 81–122. doi:10.1016/S0010-8545(00)80009-0

Goswami, T. K., Chakravarthi, B.V. S. K., Roy, M., Karande, A. A., & Chakravarty, A. R.

(2011). Ferrocene–Conjugated L–Tryptophan Copper(II) Complexes of Phenanthroline Bases Showing DNA Photocleavage Activity and Cytotoxicity. *Inorganic Chemistry*, 50, 8452–8464. doi:10.1021/ic201028e

Gou, Y., Li, J., Fan, B., Xu, B., Zhou, M., & Yang, F. (2017). Structure and biological properties of mixed–ligand Cu(II) Schiff base complexes as potential anticancer agents. *European Journal of Medicinal Chemistry*, 134, 207–217.

doi:10.1016/j.ejmech.2017.04.026

Gu, Z., Li, Y., Ma, S., Li, S., Zhou, G., Ding, S., Zhang, J., Wang, S., & Zhou, C. (2017). Synthesis, cytotoxic evaluation and DNA binding study of 9–fluoro–6H–indolo[2,3–b]quinoxaline derivatives. *RSC Advances*, 7, 41869–41879. doi:10.1039/C7RA08138C

Hameed A., Rashida, M. al–, Uroos, M., Ali, S. A., & Khan, K. M. (2017). Schiff bases in medicinal chemistry: a patent review (2010–2015). *Expert Opinion on Therapeutic Patents*, 27, 63–79. doi:10.1080/13543776.2017.1252752

Hassan, E. A., Hassan, M. L., Moorefield, C. N., & Newkome G. R. (2015). New supramolecular metallo–terpyridine carboxymethyl cellulose derivatives with antimicrobial properties. *Carbohydrate Polymers*, 116, 2–8.

doi:10.1016/j.carbpol.2014.06.056

Hranjec, M., Starčević, K., Pavelić, S.K., Lučin, P., Pavelić, K., & Zamola, G. K. (2011). Synthesis, spectroscopic characterization and antiproliferative evaluation *in vitro* of novel Schiff Bases related to benzimidazoles. *European Journal of Medicinal Chemistry*, 46, 2274–2279. doi:10.1016/j.ejmech.2011.03.008.

<http://www.fda.gov/Drugs/DevelopmentApprovalProcess/DrugInnovation/default.htm>.

Jadhao, M., Das, C., Rawat, A., Kumar, H., Joshi, R., Maiti, S., & Ghosh, S. K., (2017).

Development of multifunctional heterocyclic Schiff base as a potential metal chelator: a comprehensive spectroscopic approach towards drug discovery.

*Journal of Biological Inorganic Chemistry*, 22, 47–59. doi: 10.1007/s00775-016-1407-2

Jana, S., Dalapati, S., & Guchhait, N. (2012) Proton Transfer Assisted Charge Transfer

Phenomena in Photochromic Schiff Bases and Effect of  $-NEt_2$  Groups to the Anil Schiff Bases. *Journal of Physical Chemistry A*, 116, 10948–10958. doi:10.1021/jp3079698

Jarrahpour A., Fathi, J., Mimouni, M., Hadda, T. B., Sheikh, J., Chohan, Z., & Parvez, A.

(2012). Petra, Osiris and Molinspiration (POM) together as a successful support in drug design: antibacterial activity and biopharmaceutical characterization of some azo Schiff bases. *Medicinal Chemistry Research*, 21, 1984–1990. doi:10.1007/s00044-011-9723-0

Jawoor, S. S., Patil, S. A., & Toragalmath S.S. (2018). Synthesis and characterization of

heteroleptic Schiff base transition metal complexes: a study of anticancer, antimicrobial, DNA cleavage and anti-TB activity. *Journal of Coordination Chemistry*.

doi:10.1080/00958972.2017.1421951

Joseph, J., Nagashri, K., & Janaki G. B. (2012). Novel metal based anti-tuberculosis agent:

Synthesis, characterization, catalytic and pharmacological activities of copper

Complexes. *European Journal of Medicinal Chemistry*, 49, 151–163.

doi:10.1016/j.ejmech.2012.01.006

Kalaivani, P., Prabhakaran, R., Dallemer, F., Poornima, P., Vaishnavi, E., Ramachandran, E.,

& Natarajan, K. (2012). DNA, protein binding, cytotoxicity, cellular uptake and

antibacterial activities of new palladium(II) complexes of thiosemicarbazone ligands:

effects of substitution on biological activity. *Metallomics*, 4, 101–113.

doi:10.1039/C1MT00144B

- Khosravi, F., & Torshizi, H. M.– (2018). Antibacterial combination therapy using  $\text{Co}^{3+}$ ,  $\text{Cu}^{2+}$ ,  $\text{Zn}^{2+}$  and  $\text{Pd}^{2+}$  complexes: Their calf thymus DNA binding studies. *Journal of Biomolecular Structure and Dynamics*, 36, 1–20. doi:10.1080/07391102.2017.1281171
- Kumar, D., & Kumar Jain S. (2016). A Comprehensive Review of N–Heterocycles as Cytotoxic Agents. *Current Medicinal Chemistry*, 23, 4338–4394.
- Kumar, D., Sharma, P., Singh, H., Nepali, K., Gupta, G. K., Jain, S. K., & Kang, F. N.– (2017). The value of pyrans as anticancer scaffolds in medicinal chemistry. *RSC Advances*, 7, 36977–36999. doi:10.1039/c7ra05441f
- Kumar, D.N., Singh, B.K., Garg, B.S., & Singh P.K. (2003). Spectral studies on copper(II) complexes of biologically active glutathione. *Spectrochimica Acta Part A: Molecular and Biomolecular Spectroscopy*, 59, 1487–1496. doi:10.1016/S1386–1425(02)00303–7
- Lakowicz, J. R., & Webber, G. (1973). Quenching of Fluorescence by Oxygen: A Probe for structural Fluctuations in Macromolecules. *Biochemistry*, 12, 4161–4170. doi:10.1021/bi00745a020
- Lakshmiprabaa, J., Arunachalama, S., Solomona, R. V., Venuvanalingama, P., Riyasdeenb, A., Dhiviyac, R. & Akbarsha, M. A. (2015). Surfactant–copper(II) Schiff base complexes: synthesis, structural investigation, DNA interaction, docking studies, and cytotoxic activity. *Journal of Biomolecular Structure and Dynamics*, 33, 877–891. doi:10.1080/07391102.2014.918523
- Larsen, T. A., Goodsell, D. S., Cascio, D., Grzeskowiak, K. & Dickerson, R. E. (1989). The Structure of DAPI Bound to DNA. *Journal of Biomolecular Structure and Dynamics*, 7, 477–491. doi:10.1080/07391102.1989.10508505
- Latif, S. A. A.–, & Mohamed, A. A. (2018). Synthesis, spectroscopic characterization, first

- order nonlinear optical properties and DFT calculations of novel Mn(II), Co(II), Ni(II), Cu(II) and Zn(II) complexes with 1,3-diphenyl-4-phenylazo-5-pyrazolone ligand. *Journal of Molecular Structure*, 1153, 248–261. doi:10.1016/j.molstruc.2017.10.002
- Liu, Y. -X., Mo, H. -W., Lv, Z. -Y., F. Shen, Zhang, C. -L., Qi, Y. -Y., Mao Z. -W., & Le, X. -Yi. (2018). DNA binding, crystal structure, molecular docking studies and anticancer activity evaluation of a copper(II) complex. *Transition Metal Chemistry*. doi:10.1007/s11243-018-0211-y
- Lu, Y. J., Ou, T. M., Tan, J. H., Hou, J. Q., Shao, W. Y., Peng, D.,..... Gu, L. Q. (2008). 5-N-Methylated Quindoline Derivatives as Telomeric G-Quadruplex Stabilizing Ligands: Effects of 5-N Positive Charge on Quadruplex Binding Affinity and Cell Proliferation. *Journal of Medicinal Chemistry*, 51, 6381–6392. doi:10.1021/jm800497p
- Maass, P., Gasch, T. S., Stahl, M., & Rarey, M. (2007). Recore: A Fast and Versatile Method for Scaffold Hopping Based on Small Molecule Crystal Structure Conformations. *Journal of Chemical Information and Modeling*, 47, 390–399. doi: 10.1021/ci060094h
- Macindoe, G., Mavridis, L., Venkatraman, V., Devignes, M.-D., & Ritchie D. W. (2010). Hex Server: an FFT-based protein docking server powered by graphics processors. *Nucleic Acids Research*, 38, 445–449. doi:10.1093/nar/gkq311
- Maity, B., Roy, M., Banik, B., Majumdar, R., Dighe R.R., & Chakravarty, A. R. (2010). Ferrocene-Promoted Photoactivated DNA Cleavage and Anticancer Activity of Terpyridyl Copper(II) Phenanthroline Complexes. *Organometallics*, 29, 3632–3641. doi:10.1021/om100524x
- Malik, M. A., Dar, O. A., Gull, P., Wani, M.Y., & Hashmi, A. A. (2017). Heterocyclic Schiff Base Transition Metal Complexes in Antimicrobial and Anticancer chemotherapy. *Medicinal Chemistry Communication*. doi:10.1039/C7MD00526A

Mandegani, Z., Asadi, Z., Asadi, M., Heidari, H. R.K., & Rastegari, B. (2016).

Synthesis, characterization, DNA binding, cleavage activity, cytotoxicity and molecular docking of new nano water-soluble  $[M(5-CH_2PPh_3-3,4-salpyr)](ClO_4)_2$  (M = Ni, Zn) complexes. *Dalton Transaction*, 45, 6592–6611. doi:10.1039/C5DT04788A

Manikandamathavan, V.M., Weyhermüller, T., Parameswari, R.P., Sathishkumar, M.,

Subramaniana, V., & Nair, B. U. (2014). DNA/protein interaction and cytotoxic activity of imidazole terpyridine derived Cu(II)/Zn(II) metal complexes. *Dalton Transaction*, 43, 13018–13031. doi:10.1039/C4DT01378F

Manjunath, M., Kulkarni, A.D., Bagihalli, G.B., Malladi, S., & Patil, S.A. (2017).

Bio-important antipyrine derived Schiff Bases and their transition metal complexes: Synthesis, spectroscopic characterization, antimicrobial, anthelmintic and DNA cleavage investigation. *Journal of Molecular Structure*, 1127, 314–321.  
doi:10.1016/j.molstruc.2016.07.123

McGivern, T.J.P., Afsharpour, S., & Marmion, C.J. (2017). Copper complexes as artificial DNA

Metallonucleases: From Sigman's reagent to next generation anti-cancer agent. *Inorganica Chimica Acta*. doi:10.1016/j.ica.2017.08.043

Mendiguchia, B. S., Pucci, D., Mastropietro, T.F., Ghedini, M., & Crispini, A. (2013).

Nonclassical anticancer agents: on the way to water soluble zinc(II) heteroleptic complexes. *Dalton Transaction*, 42, 6768–6774. doi:10.1039/C3DT50367D

Nagababu, P., Barui A. K., Thulasiram B., Devi, C. S., Satyanarayana, S., Patra, C. R., &

Sreedhar, B. (2015). Antiangiogenic Activity of Mononuclear Copper(II) Polypyridyl Complexes for the Treatment of Cancers. *Journal of Medicinal Chemistry*, 58, 5226–5241. doi:10.1021/acs.jmedchem.5b00651

Nakamoto, K. (1986). Infrared and Raman spectra of inorganic and coordination compounds. Wiley Online Library.

Noolvi, M.N., Patel, H.M., & Kaur, M. (2012). Benzothiazoles: search for anticancer agents, *European Journal of Medicinal Chemistry*, 54, 447–462.  
doi:10.1016/j.ejmech.2012.05.028

Orojloo, M., Zolgharnein, P., Solimannejad, M., & Amani S. (2017). Synthesis and characterization of cobalt (II), nickel (II), copper (II) and zinc (II) complexes derived from two Schiff base ligands: spectroscopic, thermal, magnetic moment, electrochemical and antimicrobial studies. *Inorganica Chimica Acta*, 467, 227–237.  
doi:10.1016/j.ica.2017.08.016

Parvez, A., Meshram, J., Tiwari, V., Sheik, J., Dongre, R., Youssoufi, M.H., & Hadda T. B. (2010). Pharmacophores modeling in terms of prediction of theoretical physico-chemical properties and verification by experimental correlations of novel coumarin derivatives produced via Betti's protocol. *European Journal of Medicinal Chemistry*, 45, 4370–4378. doi: 10.1016/j.ejmech.2010.06.004

Protaa, A. E., Bargstena, K., Diazb, J. F., Marshc, M., Cuevasd, C., Linigere, M., & Steinmetz M.O. (2014). A new tubulin-binding site and pharmacophore for microtubule-destabilizing anticancer drugs. *Proceedings of the National Academy of Sciences, USA*, 111, 13817–13821. doi:10.1073/pnas.1408124111

Qiao, X., Ma, Z.-Y., Xie, C. -Z., Xue, F., Zhang, Y. -W., Xu, J. -Y., & Yan S.-P. (2011). Study on potential antitumor mechanism of a novel Schiff Base copper(II) complex: Synthesis, crystal structure, DNA binding, cytotoxicity and apoptosis induction activity. *Journal of Inorganic Biochemistry*, 105, 728–737.

doi:10.1016/j.jinorgbio.2011.01.004

Racane, L., Pavelic, S.K., Nhili, R., Depauw, S., Constant, C. P.–, Ratkaj, I. & Zamola G. K.– (2013). New anticancer active and selective phenylene– bisbenzothiazoles: synthesis, antiproliferative evaluation and DNA binding. *European Journal of Medicinal Chemistry*, 63, 882–891. doi:10.1016/j.jinorgbio.2011.01.004

Renfrew., A. K. (2014). Transition metal complexes with bioactive ligands: mechanisms for selective ligand release and applications for drug delivery. *Metallomics*, 6, 1324–1335. doi:https://doi.org/10.1039/C4MT00069B

Santini, C., Pellei, M., Gandin, V., Porchia, M., Tisato, F., & Marzan, C. (2014). Advances in Copper Complexes as Anticancer Agents. *Chemical Reviews*, 114, 815–862. doi: 10.1021/cr400135x

Satyanarayana, S., Dabrowiak, J. C., Chaires & J. B. (1993). Tris(phenanthroline)ruthenium(II) enantiomer interactions with DNA: mode and specificity of binding. *Biochemistry*, 32, 2573–2584. doi:10.1021/bi00061a015

Shaik, T. B., Hussaini, S. M. A., Nayak, V. L., Sucharitha, M. L., Malik, M. S., & Kamal, A. (2017). Rational design and synthesis of 2–anilinopyridinyl–benzothiazole Schiff bases as antimitotic agents. *Bioorganic & Medicinal Chemistry Letters*, 27, 2549–2558. doi:10.1016/j.bmcl.2017.03.089

Shahraki, S., & Heydari A. (2017). Binding forces between a novel Schiff base palladium(II) complex and two carrier proteins: human serum albumin and  $\beta$ –lactoglobulin. *Journal of Biomolecular Structure and Dynamics*. doi:10.1080/07391102.2017.1367723

Shokohi–pour, Z., Chiniforoshan, H., Sabzalian, M. R., Esmaeili, S.–A., Abbas A., & Borojeni, M.– (2018). Cobalt (II) complex with novel unsymmetrical tetradentate Schiff base

- (ON) ligand: *In vitro* cytotoxicity studies of complex, interaction with DNA/protein, molecular docking studies, and antibacterial activity. *Journal of Biomolecular Structure and Dynamics*, *36*, 532–549. doi:10.1080/07391102.2017.1287006
- Solomon, V.R., Hu, C., & Lee, H. (2009). Hybrid pharmacophore design and synthesis of isatin–benzothiazole analogs for their anti–breast cancer activity. *Bioorganic Medicinal Chemistry*, *17*, 7585–7592. doi:10.1016/j.bmc.2009.08.068
- Tan, C.–P., Lu, Y.–Y., Ji, L.–N., & Mao, Z.–W. (2014). Metallomics insights into the programmed cell death induced by metal–based anticancer compounds. *Metallomics*, *6*, 978–995. doi:10.1039/C3MT00225J
- Tan, J., Wang, B., & Zhu, L. (2009). DNA binding, cytotoxicity, apoptotic inducing activity, and molecular modeling study of quercetin zinc(II) complex. *Bioorganic and Medicinal Chemistry*, *17*, 614–62. doi:10.1016/j.bmc.2008.11.063
- Tardito, S., Bassanetti I., Bignardi, C., Elviri, L., Tegoni, M., Mucchino, C.,..... & Marchiò, L. (2011). Copper Binding Agents Acting as Copper Ionophores Lead to Caspase Inhibition and Paraptotic Cell Death in Human Cancer Cells. *Journal of American Chemical Society*, *133*, 6235–6242. doi:10.1021/ja109413c
- Trotta, E., & Paci, M.(1998). Solution structure of DAPI selectively bound in the minor groove of a DNA T·T mismatch-containing site: NMR and molecular dynamics studies. *Nucleic Acids Research*, *26*, 4706–4713. doi:10.1093/nar/26.20.4706
- Veber, D. F., Johnson, S. R., Cheng, H.–Y., Smith, B.R., Ward, K. W., & Kopple, K.D. (2002).Molecular Properties That Influence the Oral Bioavailability of Drug Candidates. *Journal of Medicinal Chemistry*, *45*, 2615–2623. doi:10.1021/jm020017n
- Wolfe, A., Shimer, G. H., Jr., & Meehan T. (1987). Polycyclic Aromatic Hydrocarbons

Physically Intercalate into Duplex Regions of Denatured DNA. *Biochemistry*, 26, 6392–6396. doi:10.1021/bi00394a013

Yu, M., Price, J. R., Jensen, P., Lovitt, C.J., Shelper, T., Duffy, S., .... Todd M. H. (2011).

Copper, Nickel, and Zinc Cyclam–Amino Acid and Cyclam–Peptide Complexes May Be Synthesized with “Click” Chemistry and Are Noncytotoxic. *Inorganic Chemistry*, 50, 12823–12835. doi:10.1021/ic2020012

Yun, B. H., Kim, J. –O., Lee, B.W., Lincoln, P., Nordèn, B., Kim, J. –M., & Kim, S. K.(2003).

Simultaneous Binding of Ruthenium(II) [(1,10–Phenanthroline)2dipyridophenazine]<sup>2+</sup> and Minor Groove Binder 4',6–Diamidino–2–phenylindole to Poly[d(A–T)<sub>2</sub>] at High Binding Densities: Observation of Fluorescence Resonance Energy Transfer Across the DNA Stem. *Journal of Physical Chemistry B*, 107, 9858–9864. doi:10.1021/jp027828n

Zhang, C.–L., Zhang, X. –M., Liu, W., Chen, S., Mao, Z.–W., & Le, X. –Y. (2017).

Synthesis, crystal structures and DNA/human serum albumin binding of ternary Cu(II) complexes containing amino acids and 6–(pyrazin–2–yl) –1,3,5–triazine–2,4–diamino. *Applied Organometallic Chemistry*, 32, 3994. doi:10.1002/aoc.3994

Zheng, K., Liu, F., Xu, X.–M., Li, Y.–T., Wua, Z.–Y., & Yan, C. –W. (2014). Synthesis,

structure and molecular docking studies of dicopper(II) complexes bridged by N–phenolato–N'–[2–(dimethylamino)ethyl] oxamide: the influence of terminal ligands on cytotoxicity and reactivity towards DNA and protein BSA. *New Journal of Chemistry*, 38,2964–2978. doi:10.1039/C4NJ00092G

## Supplementary Material

### New tailored substituted–benzothiazole Schiff base Cu(II)/Zn(II) antitumor drug entities: Effect of substituents on DNA binding profile, antimicrobial and cytotoxic activity

Sifteen Zehra<sup>a</sup>, Mohammad Shavez Khan<sup>b</sup>, Iqbal Ahmad<sup>b</sup> and Farukh Arjmand<sup>a\*</sup>

<sup>a</sup>Department of Chemistry, Aligarh Muslim University, Aligarh 202002, India

<sup>b</sup>Department of Agricultural Microbiology, Aligarh Muslim University, Aligarh 202002, India

\*Corresponding author. E-mail address: farukh\_arjmand@yahoo.co.in (F. Arjmand).

\*Corresponding author. Tel.: +91 5712703893.

#### Characterization data of Ligands L1–L3 and Complexes 1 and 2 (a–c)

[C<sub>15</sub>H<sub>12</sub>N<sub>2</sub>O<sub>2</sub>S], L1: Yield: 77%, M.P: 154°C, Anal. (%) Calc. for C<sub>15</sub>H<sub>12</sub>N<sub>2</sub>O<sub>2</sub>S<sub>2</sub>: C (62.26), H (4.25), N (9.85), Found: C (62.25), H (4.22), N (9.84). FTIR (KBr cm<sup>-1</sup>): 3435 ν(O–H), 1632 ν(HC=N), 1567 ν(C=N), 1442 ν(C–N), 872 ν(C–S). UV–vis (λ<sub>max</sub>, nm) in DMSO: 227, 260 (π–π\*), 348 (n–π\*). <sup>1</sup>H NMR (400 MHz, DMSO–d<sub>6</sub>, δ, ppm): 12.44 (OH), 9.26 (HC=N), 7.9–6.9 (Ar–H). <sup>13</sup>C NMR (100 MHz, DMSO–d<sub>6</sub>, δ, ppm): 167.49 (C=N), 158.29 (C–O), 155.94 (C–N), 134.74–116.77 (Ar–C). ESI–MS (*m/z*): 283.99 [C<sub>15</sub>H<sub>12</sub>N<sub>2</sub>O<sub>2</sub>S<sub>2</sub>]<sup>+</sup>.

[C<sub>15</sub>H<sub>11</sub>ClN<sub>2</sub>O<sub>2</sub>S], L2: Yield: 75%, M.P: 140°C, Anal. (%) Calc. for C<sub>15</sub>H<sub>11</sub>ClN<sub>2</sub>O<sub>2</sub>S<sub>2</sub>: C (56.52), H (2.48), N (8.79), Found: C (56.50), H (2.47), N (8.78). FTIR (KBr cm<sup>-1</sup>): 3433 ν(O–H), 1635 ν(HC=N), 1569 ν(C=N), 1475 ν(C–N), 871 ν(C–S). UV–vis (λ<sub>max</sub>, nm) in DMSO: 225, 264 (π–π\*) 341 (n–π\*). <sup>1</sup>H NMR (400 MHz, DMSO–d<sub>6</sub>, δ, ppm): 11.12 (OH), 9.43 (HC=N), 7.99–6.98 (Ar–H). <sup>13</sup>C NMR (100 MHz, DMSO–d<sub>6</sub>, δ, ppm): 167.17 (C=N), 149.31 (C–O), 148.04 (C–N), 135.33–116.89 (Ar–C). ESI–MS (*m/z*): 319.31[C<sub>15</sub>H<sub>11</sub>ClN<sub>2</sub>O<sub>2</sub>S<sub>2</sub>+H]<sup>+</sup>.

[C<sub>15</sub>H<sub>11</sub>FN<sub>2</sub>O<sub>2</sub>S], L3: Yield: 80%, M.P: 144°C, Anal. (%) Calc. for C<sub>15</sub>H<sub>11</sub>FN<sub>2</sub>O<sub>2</sub>S<sub>2</sub>: C (59.59), H (2.67), N (9.27), Found: C (59.49), H (2.65), N (9.25). FTIR (KBr cm<sup>-1</sup>): 3434 ν(O–H), 1633 ν(HC=N), 1568 ν(C=N), 1442 ν(C–N), 870 ν(C–S). UV–vis (λ<sub>max</sub>, nm) in DMSO: 226, 262

( $\pi-\pi^*$ ), 345 ( $n-\pi^*$ ).  $^1\text{H}$  NMR (400 MHz,  $\text{DMSO}-d_6$ ,  $\delta$ , ppm): 11.50 (OH), 9.36 (HC=N), 7.93–6.92 (Ar–H).  $^{13}\text{C}$  NMR (100 MHz,  $\text{DMSO}-d_6$ ,  $\delta$ , ppm): 166.51 (C=N), 147.82 (C–O), 147.61 (C–N), 134.96–106.88 (Ar–C). ESI–MS ( $m/z$ ): 303.4 [ $\text{C}_{15}\text{H}_{11}\text{FN}_2\text{O}_2\text{S}_2$ ] $^+$ .

Complex [ $\text{C}_{30}\text{H}_{22}\text{Cl}_2\text{CuN}_5\text{O}_7\text{S}_2$ ], **1a**: Yield: %, M.P: 215 °C, Anal. (%) Calc. for  $\text{C}_{30}\text{H}_{22}\text{Cl}_2\text{CuN}_5\text{O}_7\text{S}_2$ : C (52.10), H (2.12), N (10.10), Found: C (52.00), H (2.11), N (10.09).

FTIR (KBr  $\text{cm}^{-1}$ ): 1640  $\nu(\text{HC}=\text{N})$ , 1526  $\nu(\text{C}=\text{N})$ , 1458  $\nu(\text{C}-\text{N})$ , 522  $\nu(\text{M}-\text{O})$ , 467  $\nu(\text{M}-\text{N})$ .

UV–vis ( $\lambda_{\text{max}}$ , nm) in DMSO: 270 ( $\pi-\pi^*$ ), 364 ( $n-\pi^*$ ), 521 (d–d). ESI–MS ( $m/z$ ): 691.08

[ $\text{C}_{30}\text{H}_{22}\text{Cl}_2\text{CuN}_5\text{O}_7\text{S}_2$ ] $^+$ .

Complex [ $\text{C}_{30}\text{H}_{20}\text{Cl}_2\text{CuN}_5\text{O}_7\text{S}_2$ ], **1b**: Yield: 75%, M.P: 217°C, Anal. (%) Calc. for

$\text{C}_{30}\text{H}_{20}\text{Cl}_2\text{CuN}_5\text{O}_7\text{S}_2$ : C (47.20), H (2.52), N (9.12), Found: C (47.29), H (2.51), N (9.12). FTIR

(KBr  $\text{cm}^{-1}$ ): 1610  $\nu(\text{HC}=\text{N})$ , 1542  $\nu(\text{C}=\text{N})$ , 1421  $\nu(\text{C}-\text{N})$ , 509  $\nu(\text{M}-\text{O})$ , 446  $\nu(\text{M}-\text{N})$ . UV–vis

( $\lambda_{\text{max}}$ , nm) in DMSO: 272 ( $\pi-\pi^*$ ), 367 ( $n-\pi^*$ ), 529 (d–d). ESI–MS ( $m/z$ ): 758.75

[ $\text{C}_{30}\text{H}_{20}\text{Cl}_2\text{CuN}_5\text{O}_7\text{S}_2$ ] $^+$ .

Complex [ $\text{C}_{30}\text{H}_{20}\text{F}_2\text{CuN}_5\text{O}_7\text{S}_2$ ], **1c**: Yield: 75%, M.P: 220°C, Anal. (%) Calc. for

$\text{C}_{30}\text{H}_{20}\text{F}_2\text{CuN}_5\text{O}_7\text{S}_2$ : C (51.46), H (2.17), N (8.0), Found: C (51.80), H (2.27), N (8.80). FTIR

(KBr  $\text{cm}^{-1}$ ): 1609  $\nu(\text{HC}=\text{N})$ , 1529  $\nu(\text{C}=\text{N})$ , 1470  $\nu(\text{C}-\text{N})$ , 465  $\nu(\text{M}-\text{O})$ , 420  $\nu(\text{M}-\text{N})$ . UV–vis

( $\lambda_{\text{max}}$ , nm) in DMSO: 275 ( $\pi-\pi^*$ ), 361 ( $n-\pi^*$ ), 526 (d–d). ESI–MS ( $m/z$ ): 730.77

[ $\text{C}_{30}\text{H}_{20}\text{F}_2\text{CuN}_5\text{O}_7\text{S}_2$ ].

Complex [ $\text{C}_{30}\text{H}_{22}\text{N}_4\text{O}_4\text{S}_2\text{Zn}$ ], **2a**: Yield: %, M.P: 218°C, Anal. (%) Calc. for  $\text{C}_{30}\text{H}_{22}\text{N}_4\text{O}_4\text{S}_2\text{Zn}$ :

C (57.10), H (2.51), N (8.85), Found: C (57.00), H (2.50), N (8.84). FTIR (KBr  $\text{cm}^{-1}$ ): 1606

$\nu(\text{HC}=\text{N})$ , 1542  $\nu(\text{C}=\text{N})$ , 1470  $\nu(\text{C}-\text{N})$ , 527  $\nu(\text{M}-\text{O})$ , 462  $\nu(\text{M}-\text{N})$ .  $^1\text{H}$  NMR (400 MHz,

$\text{DMSO}-d_6$ , ppm): 8.15 (HC=N), 7.77–6.99 (Ar–H), 2.53 ( $\text{CH}_2$ ).  $^{13}\text{C}$  NMR (100 MHz,

DMSO-*d*<sub>6</sub>, ppm): 168.25 (C=N), 151.68 (C-N), 120.26 (Ar-C). UV-vis ( $\lambda_{\text{max}}$ , nm) in DMSO: 269 ( $\pi-\pi^*$ ), 354 ( $n-\pi^*$ ). ESI-MS (*m/z*): 740 [ $\text{C}_{30}\text{H}_{22}\text{N}_4\text{O}_4\text{S}_2\text{Zn}$ ]<sup>+</sup>.

Complex [ $\text{C}_{30}\text{H}_{20}\text{Cl}_2\text{N}_4\text{O}_4\text{S}_2\text{Zn}$ ], **2b**: Yield: %, M.P: 212°C, Anal. (%) Calc. for

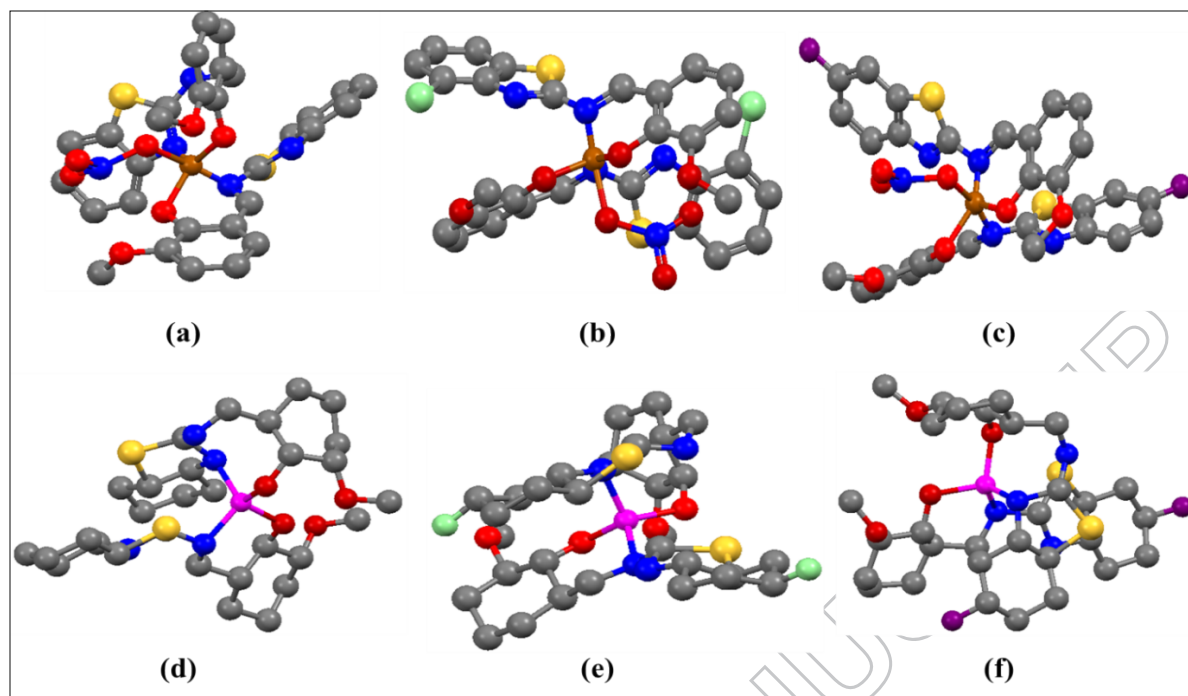
$\text{C}_{30}\text{H}_{20}\text{Cl}_2\text{N}_4\text{O}_4\text{S}_2\text{Zn}$ : C (51.40), H (2.82), N (7.90), Found: C (51.29), H (2.85), N (7.89). FTIR (KBr  $\text{cm}^{-1}$ ): 1645  $\nu(\text{HC}=\text{N})$ , 1542  $\nu(\text{C}=\text{N})$ , 1452  $\nu(\text{C}-\text{N})$ , 540  $\nu(\text{M}-\text{O})$ , 440  $\nu(\text{M}-\text{N})$ . <sup>1</sup>H NMR (400 MHz, DMSO-*d*<sub>6</sub>, ppm): 8.17 (HC=N), 7.96–6.52 (Ar-H), 2.52 (CH<sub>2</sub>). <sup>13</sup>C NMR (100 MHz, DMSO-*d*<sub>6</sub>, ppm): 148.17 (C=N), 148.17 (C-N), 126.42–119.18 (Ar-C), 28.86 (CH<sub>2</sub>).

UV-vis ( $\lambda_{\text{max}}$ , nm) in DMSO: 274 ( $\pi-\pi^*$ ), 356 ( $n-\pi^*$ ). ESI-MS (*m/z*): 700.79

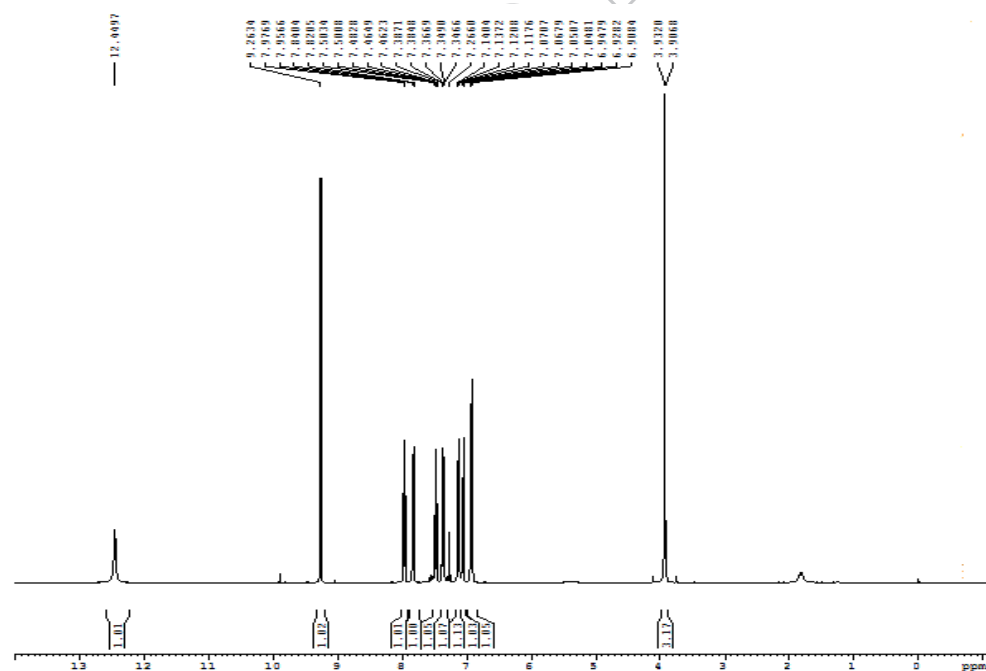
[ $\text{C}_{30}\text{H}_{20}\text{Cl}_2\text{N}_4\text{O}_4\text{S}_2\text{Zn}$ ]<sup>+</sup>.

Complex [ $\text{C}_{30}\text{H}_{20}\text{F}_2\text{N}_5\text{O}_7\text{S}_2\text{Zn}$ ], **2c**: Yield: 70%, M.P: 210°C, Anal. (%) Calc. for

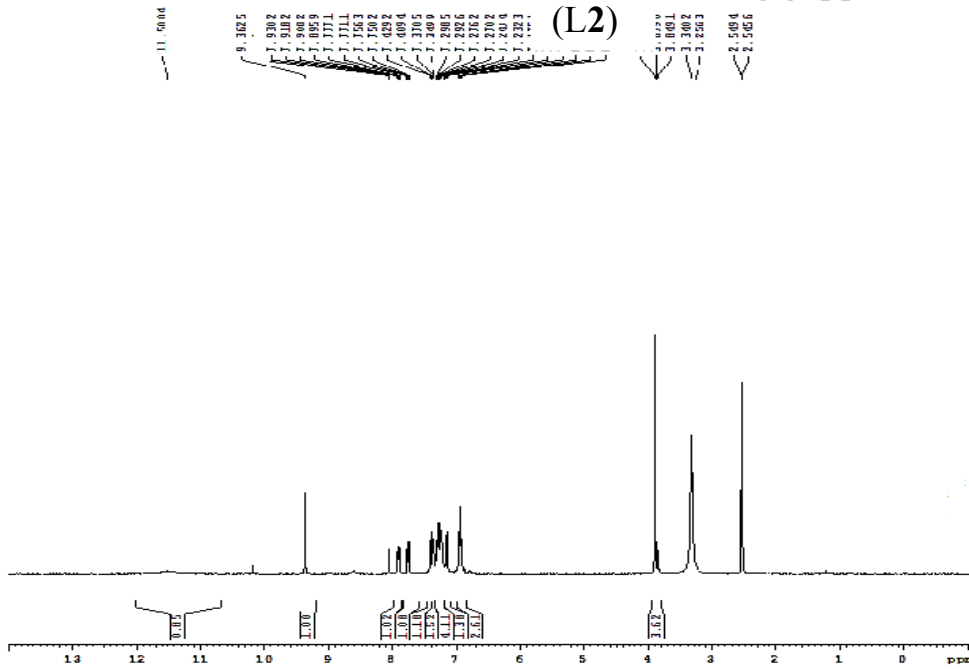
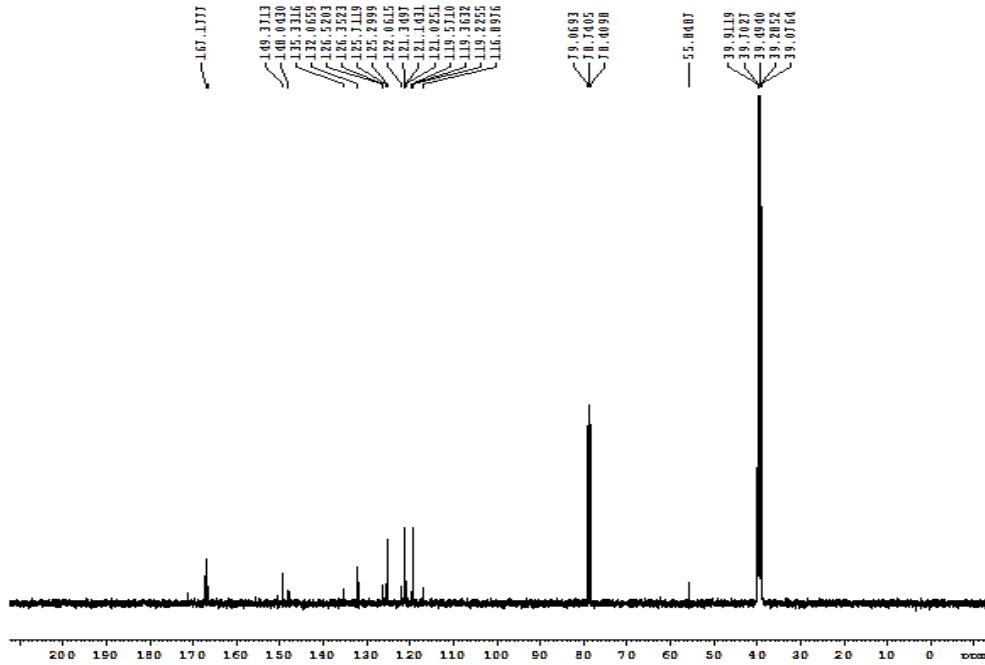
$\text{C}_{30}\text{H}_{20}\text{F}_2\text{N}_5\text{O}_7\text{S}_2\text{Zn}$ : C (44.96), H (2.02), N (6.99), Found: C (44.27), H (2.245), N (6.29). FTIR (KBr  $\text{cm}^{-1}$ ): 1606  $\nu(\text{HC}=\text{N})$ , 1542  $\nu(\text{C}=\text{N})$ , 1442  $\nu(\text{C}-\text{N})$ , 542  $\nu(\text{M}-\text{O})$ , 425  $\nu(\text{M}-\text{N})$ . <sup>1</sup>H NMR (400 MHz, DMSO-*d*<sub>6</sub>, ppm): 9.29 (HC=N), 7.7–6.4 (Ar-H), 2.6 (CH<sub>2</sub>). <sup>13</sup>C NMR (100 MHz, DMSO-*d*<sub>6</sub>, ppm): 167.06 (C=N), 156.02 (C-N), 148.70–107.68 (Ar-C), 22.41 (CH<sub>2</sub>). UV-vis ( $\lambda_{\text{max}}$ , nm) in DMSO: 272 ( $\pi-\pi^*$ ), 355 ( $n-\pi^*$ ). ESI-MS (*m/z*): 667.1 [ $\text{C}_{30}\text{H}_{20}\text{F}_2\text{N}_5\text{O}_7\text{S}_2\text{Zn}$ ]<sup>+</sup>.

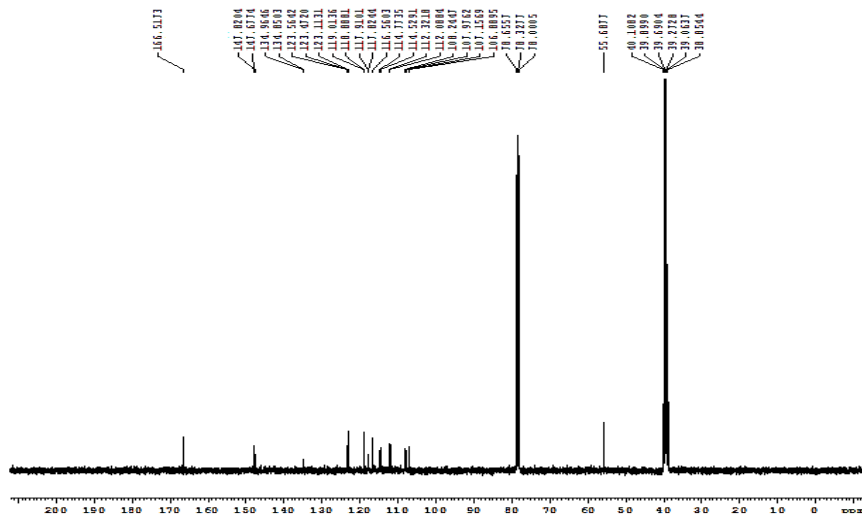


**Fig.S1.** Energy minimized 3D structure of complexes **1** and **2** (a-c) {blue = nitrogen, red = oxygen, yellow = sulphur, grey = carbon, light green = chlorine, purple = fluorine, brown = copper, pink = zinc}



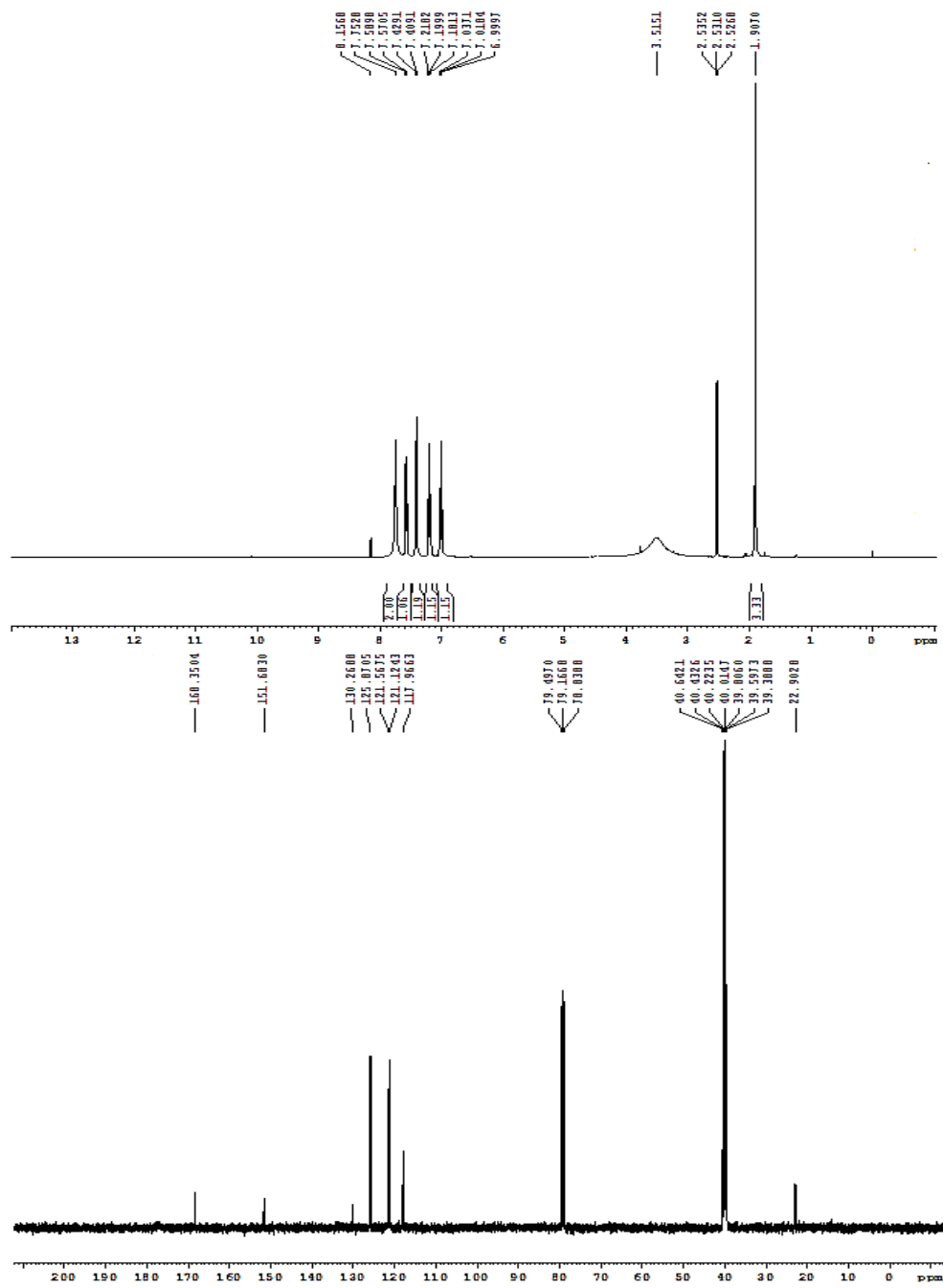






(L3)

ACCEPTED MANUSCRIPT

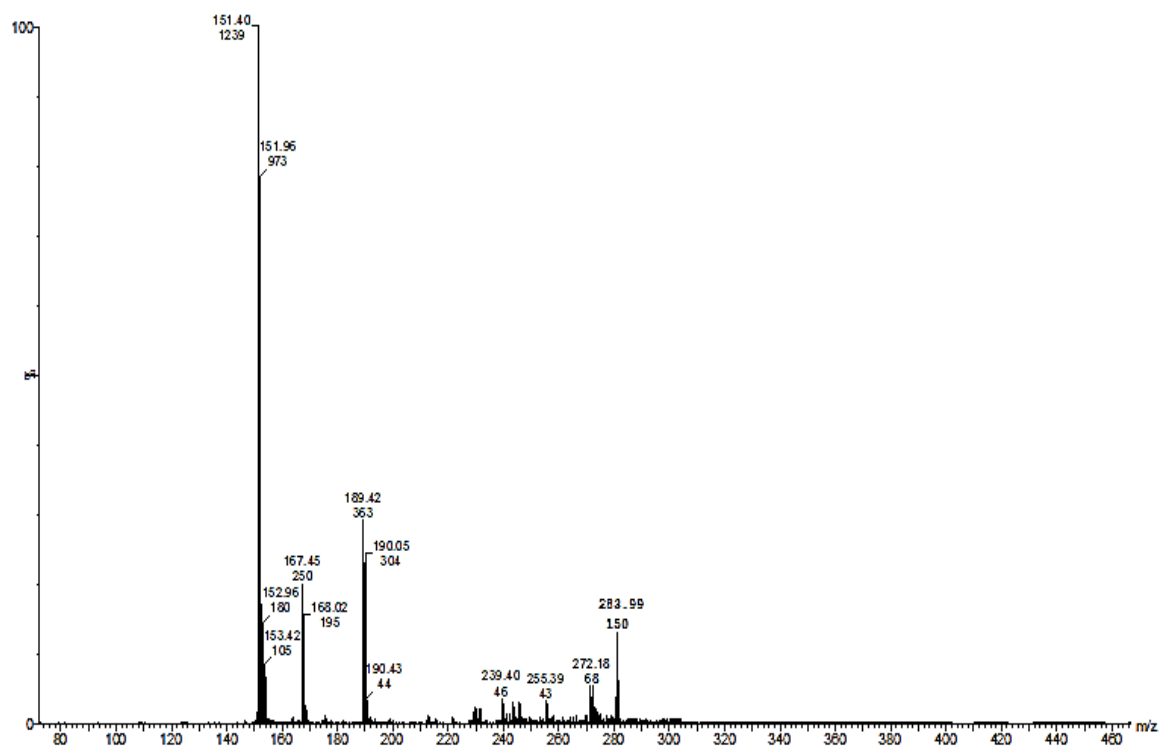


(2a)

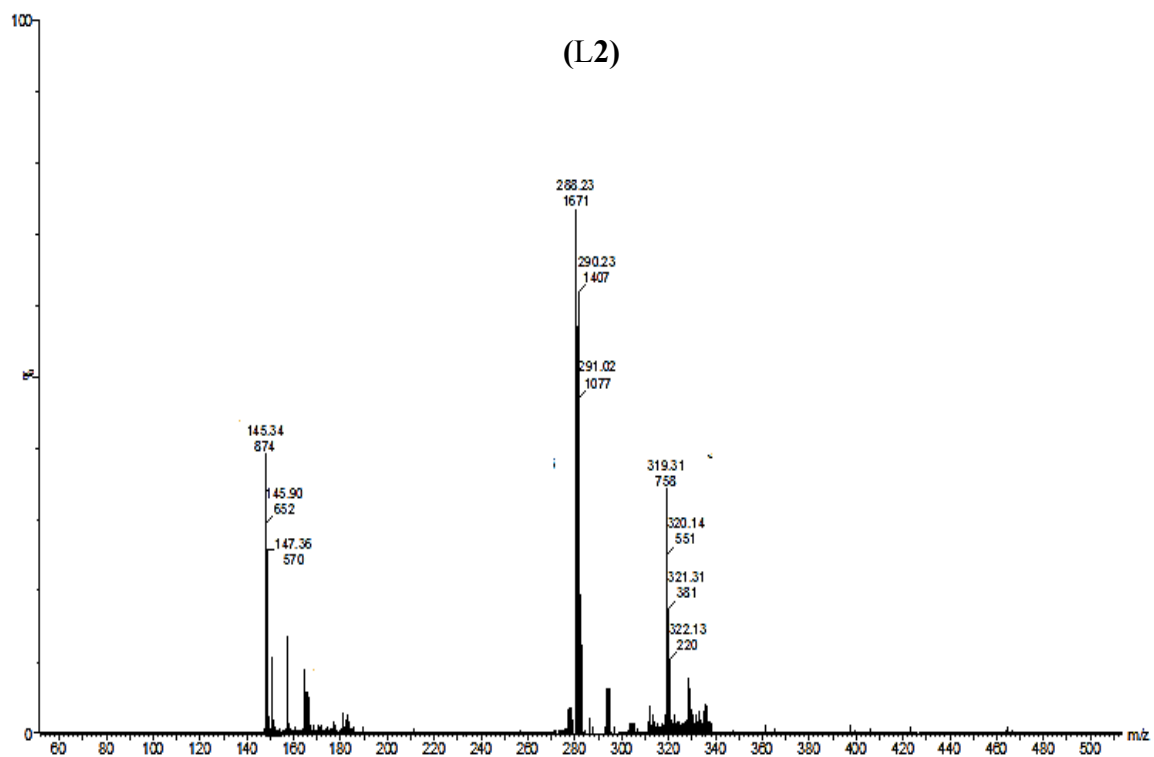




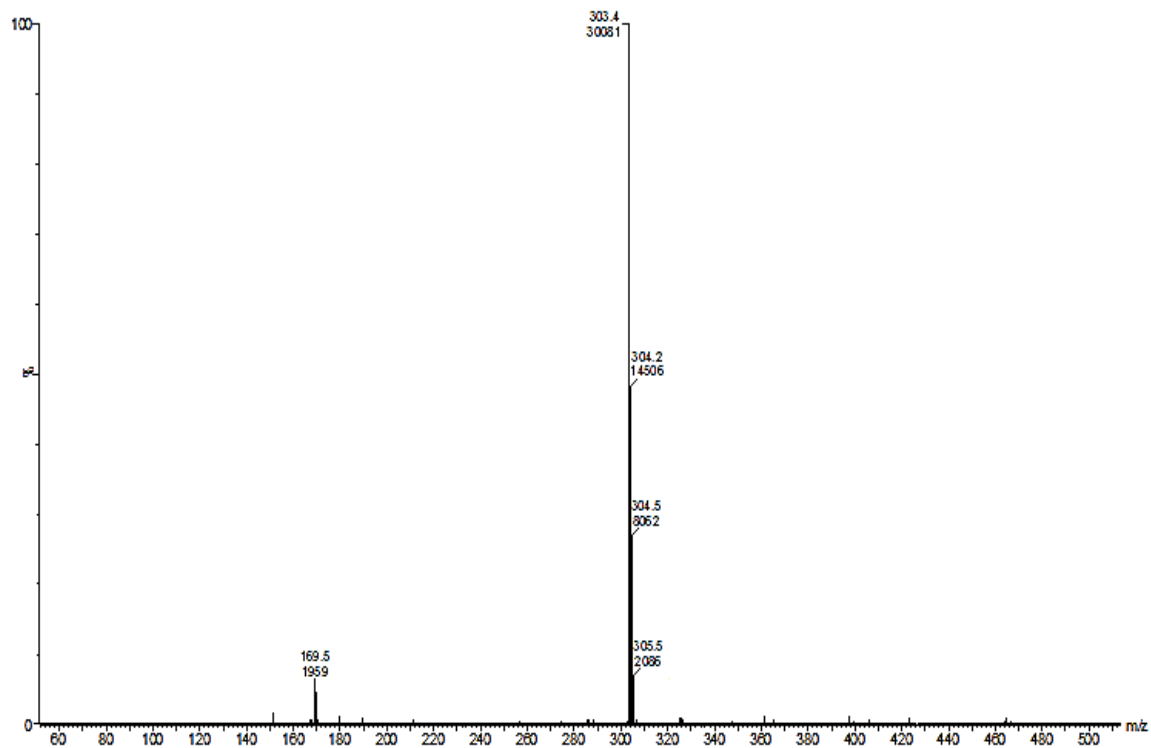
(L1)



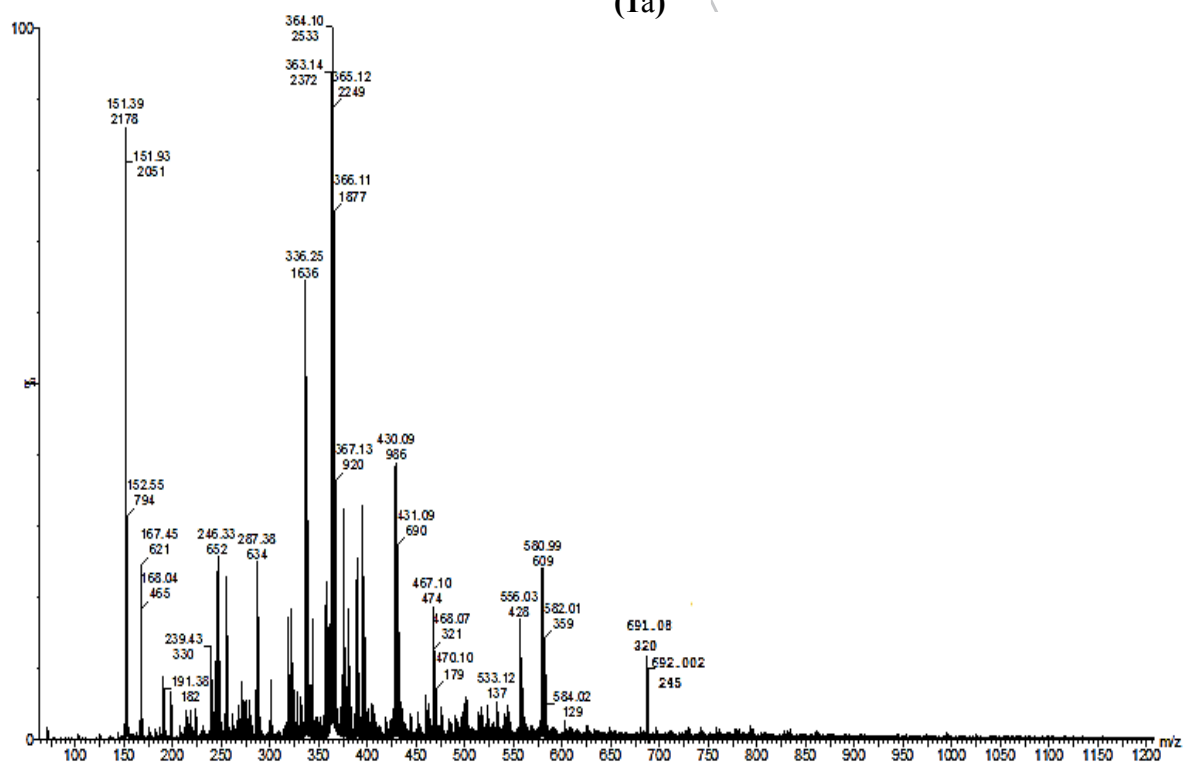
(L2)



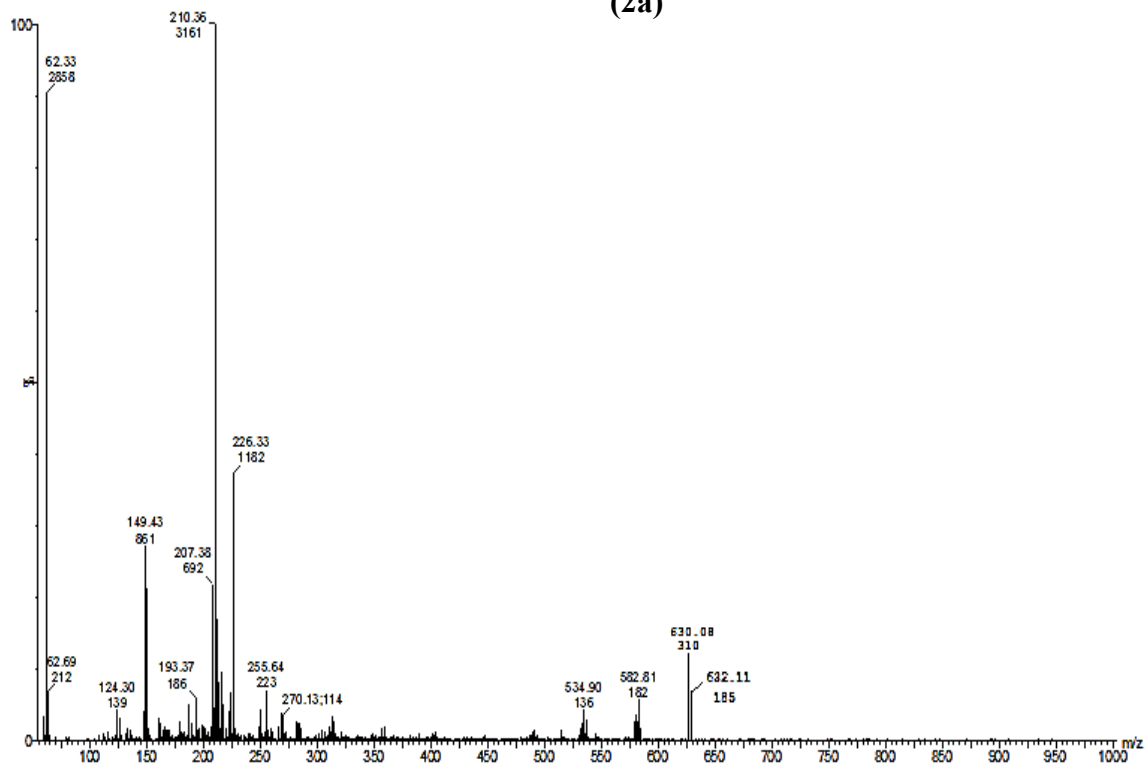
(L3)



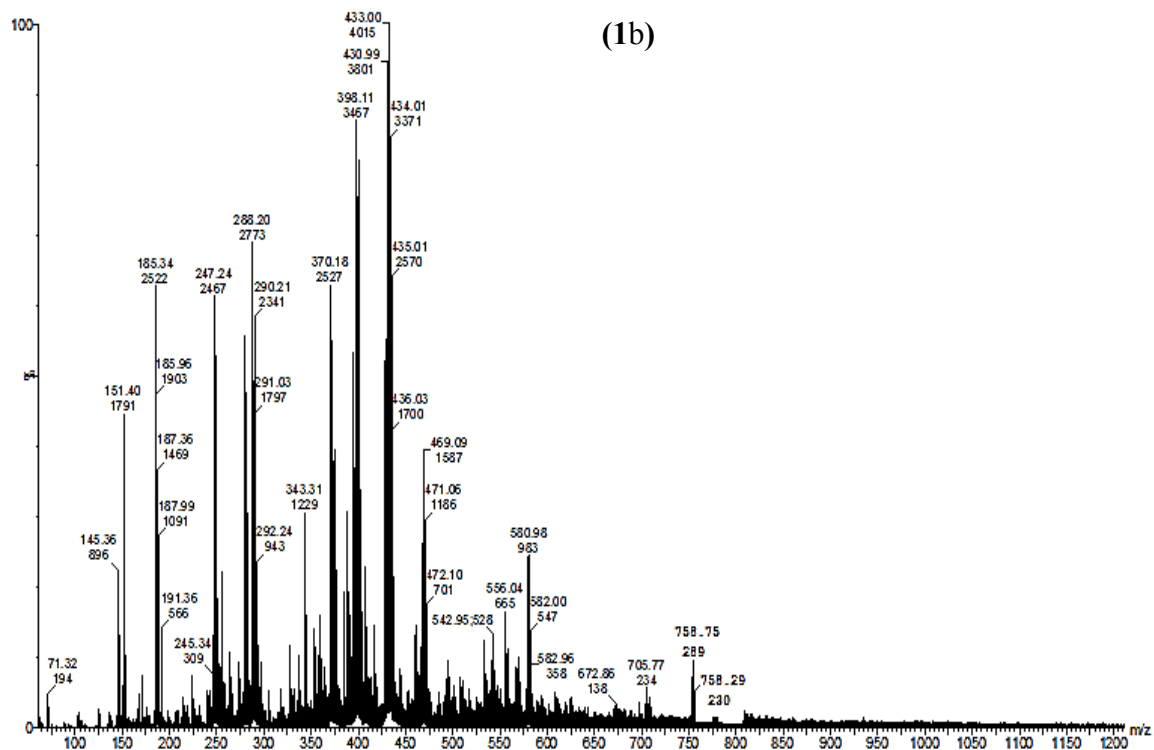
(1a)



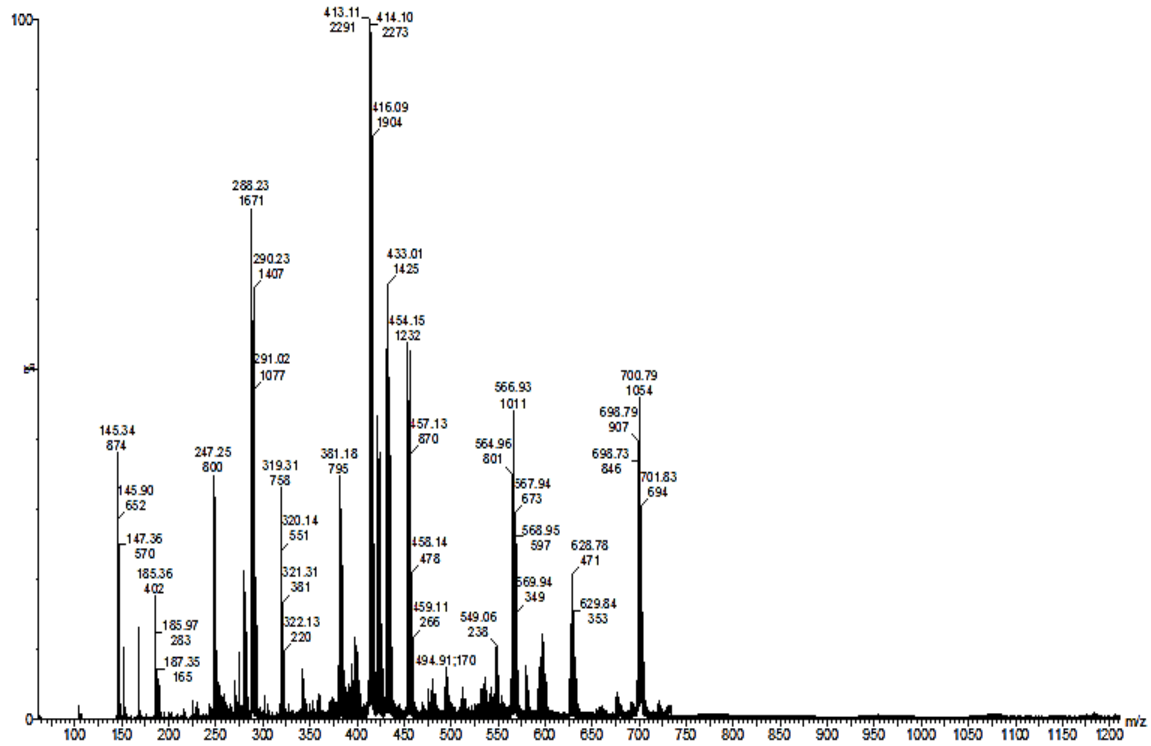
(2a)



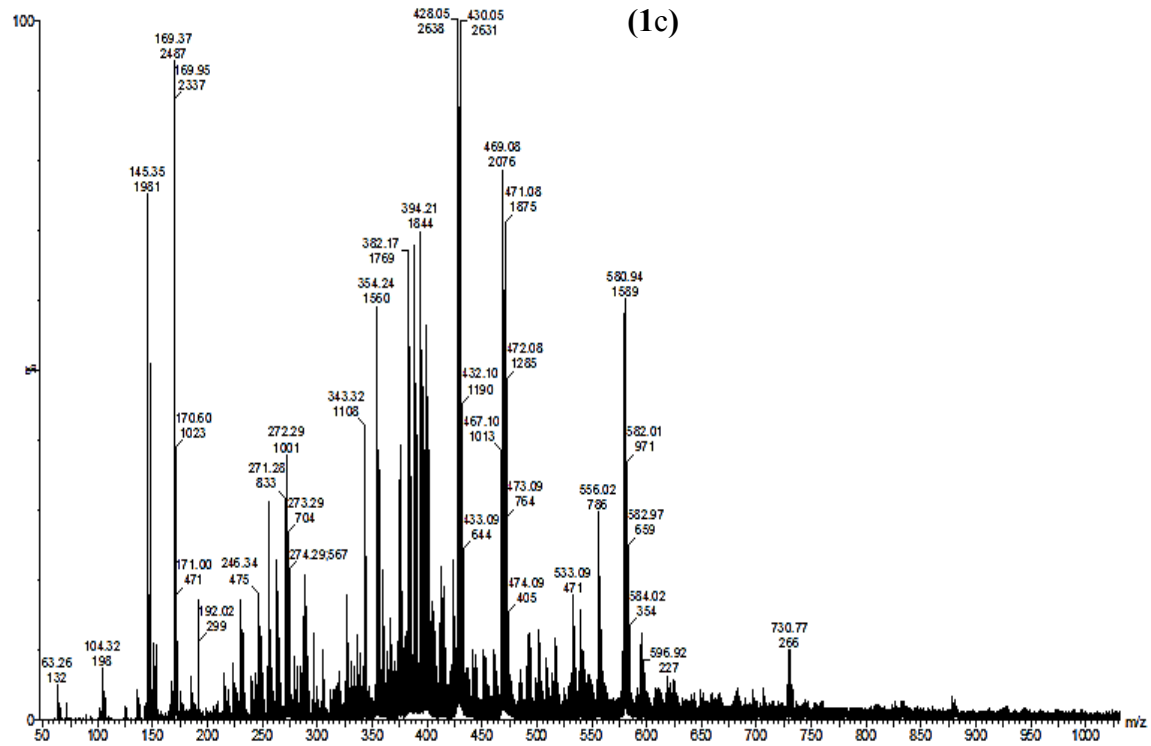
(1b)



(2b)



(1c)



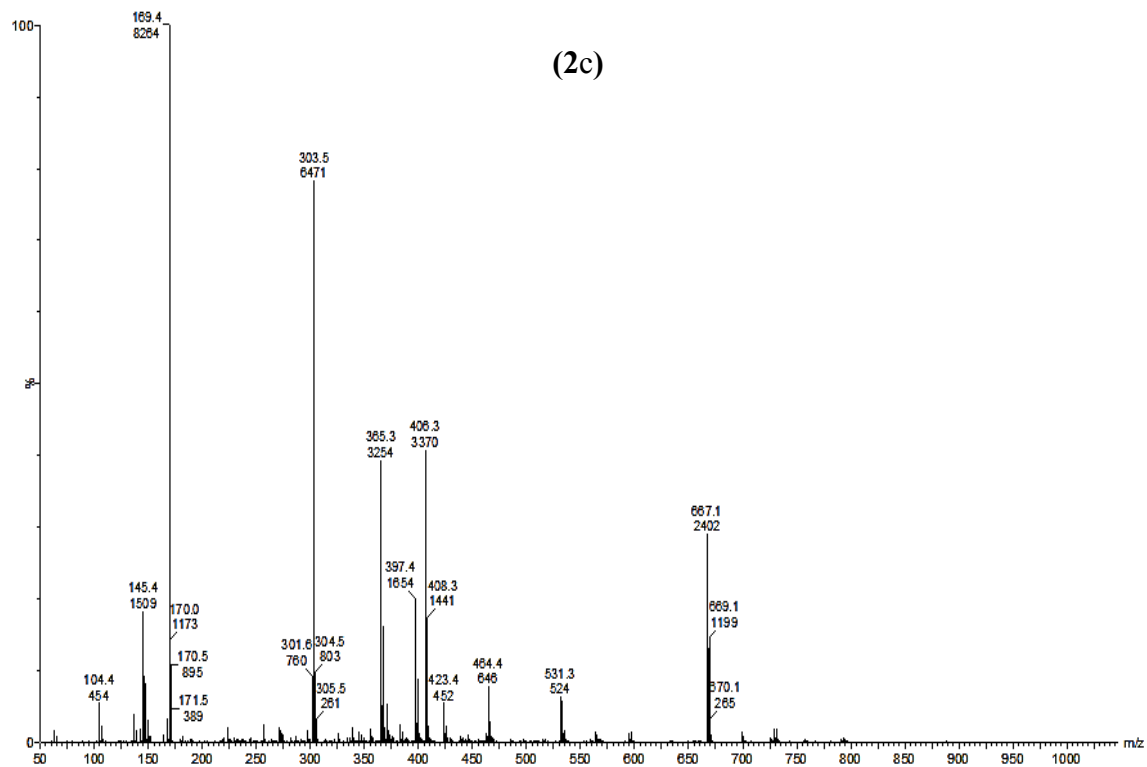


**Fig.S3.** ESI-MS spectra of ligand L1-L3 and complexes 1 and 2 (a-c).

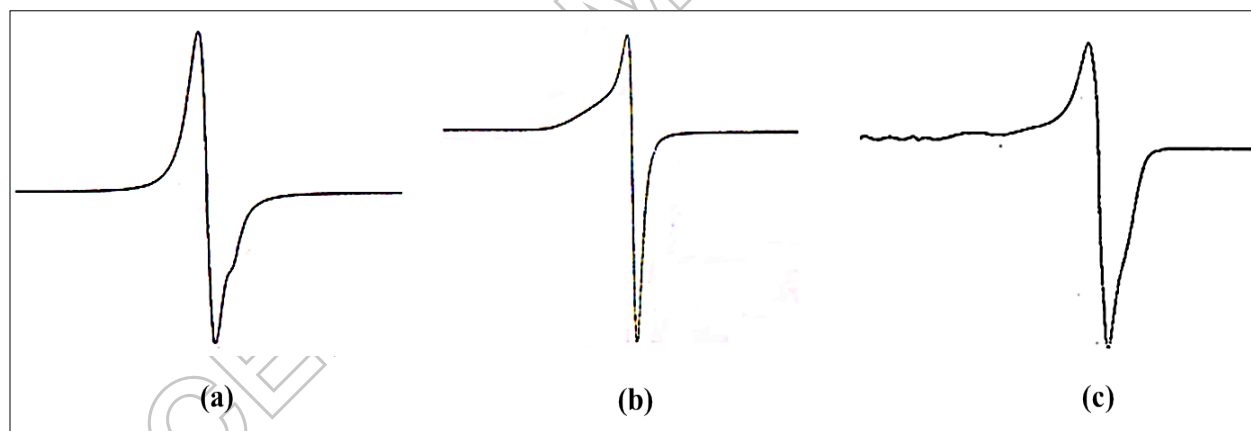


**Fig.S4.** EPR spectra of complexes 1 (a-c).

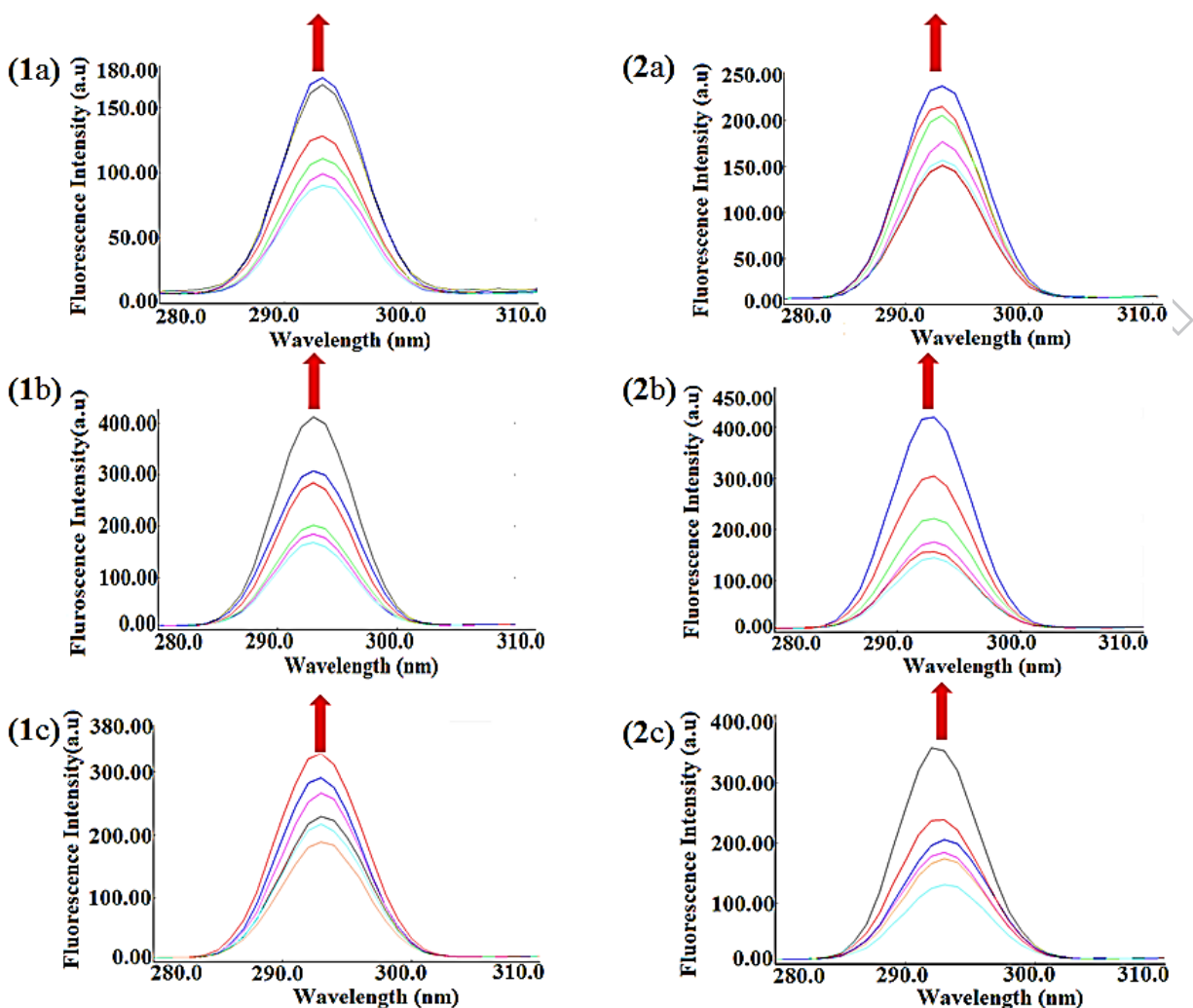
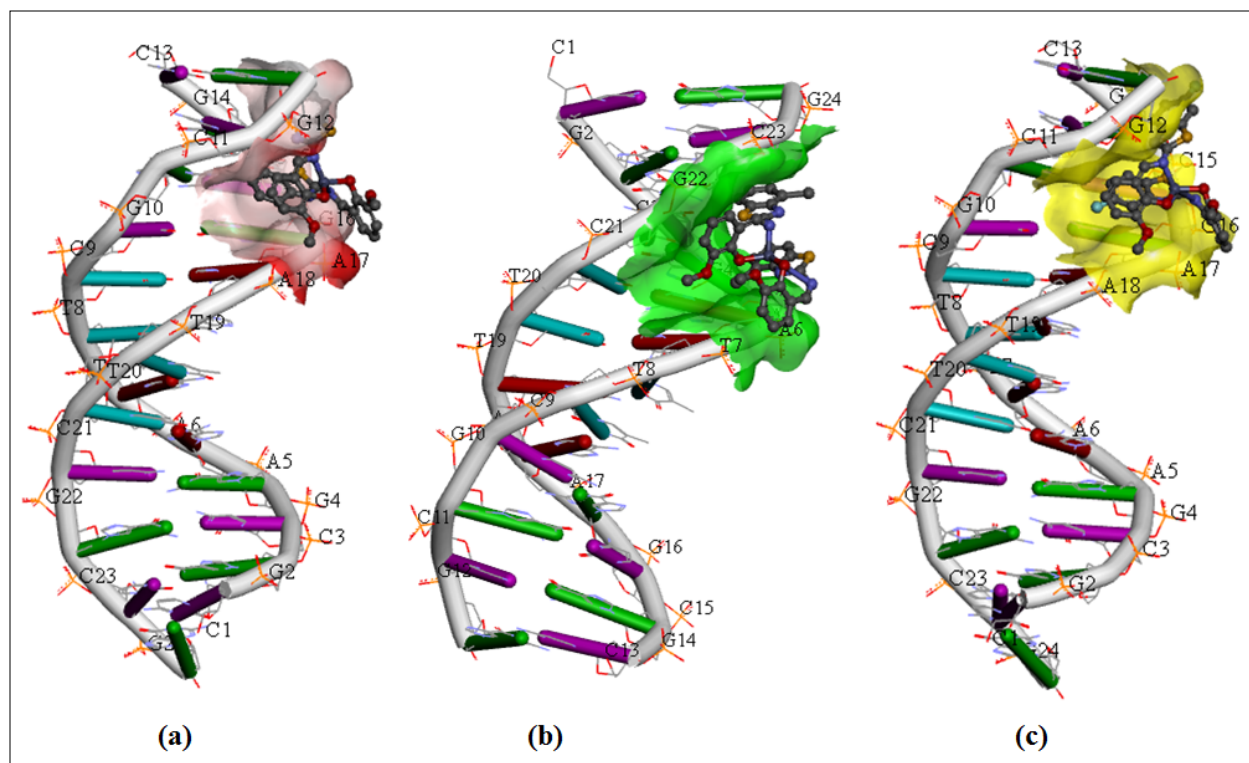


Fig.S5. Fluorescence spectra of complexes **1** and **2** (a–c) in presence of CT–DNA.

**Table S1.** Cytotoxic activity of complexes **1** and **2** (b & c) (in  $\mu\text{g/mL}$ ). TGI = Concentration of drug causing total inhibition of cell growth,  $\text{LC}_{50}$  = Concentration of drug causing 50% cell kill  
NE = Non-evaluable data

Compounds	MCF-7		MIA-PA-CA-2		HeLa		Hep-G2		A498	
	TGI	$\text{LC}_{50}$	TGI	$\text{LC}_{50}$	TGI	$\text{LC}_{50}$	TGI	$\text{LC}_{50}$	TGI	$\text{LC}_{50}$
<b>1b</b>	>80	66.5	>80	>80	NE	>80	>80	>80	>80	>80
<b>1c</b>	>80	94.2	>80	>80	NE	68.6	NE	NE	>80	>80
<b>2b</b>	>80	>80	>80	>80	NE	NE	NE	NE	>80	>80
<b>2c</b>	>80	62.3	>80	>80	NE	>80	NE	NE	>80	>80



**Fig.S6.** Molecular docked model of the complexes **2** (a–c).

ACCEPTED MANUSCRIPT